Title

Daytime and nighttime observations of chlorophyll fluorescence in Merlot grapevines: A remote sensing perspective

Author

McHugh, Devin

Publication Date

2022

Peer reviewed|Thesis/dissertation

Daytime and nighttime observations of chlorophyll fluorescence in Merlot grapevines: A remote sensing perspective

By

DEVIN P. MCHUGH
THESIS

Submitted in partial satisfaction of the requirements for the degree of

MASTER OF ARTS

in

Geography

in the

OFFICE OF GRADUATE STUDIES

of the

UNIVERSITY OF CALIFORNIA

DAVIS

Approved:

Troy Magney, Chair

Andrew McElrone

Yufang Jin

Committee in Charge

2022

Table of Contents

Abstract ***iii***

Statement of Purpose ***v***

Introduction ***1***

Methods ***7***

Study site **7**

Tower-based SIF system **7**
Data processing and normalization 9

Eddy Covariance **12**

Canopy-based LEDIF system **12**
Data processing and normalization 14

Statistical analysis **18**

Results ***19***

Canopy-based LEDIF system timeseries **19**

Eddy covariance **21**

Tower-based PhenoSpec system timeseries **22**

Linear models for canopy-based LEDIF, tower-based PhenoSpec, and eddy covariance systems **24**

Random forest models for tower-based PhenoSpec and eddy covariance systems **26**

Discussion ***30***

Canopy-based LEDIF system **30**
Design and setup takeaways 30
Data and results 31
Strengths and limitations 34

Tower-based PhenoSpec system **35**
Design and setup takeaways 35
Data and results compared with canopy-based LEDIF system 36
Strengths and limitations 40

Assessment of project goals **42**

Conclusion ***44***

Supplemental Figures ***46***

References ***51***

Abstract

As a proxy for photosynthesis, ground-based and remotely-sensed measurements of solar-induced chlorophyll fluorescence (SIF) have enabled researchers to quantitatively interpret photochemical activity of plants on a variety of scales. However, measuring SIF can be difficult, requiring fine-resolution spectral information and meticulous processing to tease apart fluorescence emissions from reflected solar radiation. Also, current SIF measuring instruments are expensive and require a high degree of technical interpretation. In recent studies, chlorophyll fluorescence has been measured in a different way by using multispectral light-emitting diodes (LED) products at night. By removing solar radiation and instead producing artificial LED light in the blue region of the electromagnetic spectrum (400-500 nm), these studies were successful in manipulating incoming light during nighttime conditions to induce fluorescence (a process known as LEDIF). While both SIF and LEDIF measurements explore light reemission in the red and far-red regions of the spectrum, it is worth further investigating the potential of LEDIF for its ability to capture 'pure' fluorescence characteristics at a lower cost. By deploying both a red/far-red photodiode sensor (Apogee Instruments, Utah, USA) and VIS-NIR spectrometer (FLAME, Ocean Insight, Florida, USA) during nighttime conditions, this study aims to capture temporal dynamics of chlorophyll fluorescence for the duration of an entire growing season in a vineyard. This research provides insight to further understand how plants respond to variations in environmental stress, such as drought, through their spectral responses and fluorescence emissions. By capturing spectra to quantify both reflectance-based vegetation indices (NDVI, NIRv, PRI, CCI, EVI) and fluorescence emissions (SIF/LEDIF), this research aims to explore differences in their individual performances and abilities to capture grape vineyard drought in California's Central Valley. By simultaneously deploying in-situ LEDIF and SIF measuring

instruments at a single site for an entire growing season, the strengths and weaknesses of each approach can be recognized, discussed, and learned from.

Statement of Purpose

Plants are essential for sustained life on Earth. Whether as carbon sinks or providing nutrition to other organisms, plants are responsible for the facilitation of a variety of ecosystem services. Like all living things, plants have a few basic needs that must be met for their survival and prosperity. Such needs include, but are not limited to: light, oxygen, carbon dioxide, water, soil nutrition, and room to grow. To account for and quantify the many benefits plants bring forth, a vast field of ongoing research is currently being conducted to break down these basic needs of plants and hypothesizing what their unique interactions might reveal. While the looming threats of climate change (warming, drought, wildfire, etc.) present unique challenges, researchers are making great efforts to understand the complicated impacts and consequences for plants. As a master's thesis, I am interested in contributing to this greater effort to better understand how plants interact within the environment, particularly to drought in agricultural systems. My thesis research involves the implementation of field-based remote sensing techniques to capture spectral variation in grapevine plants throughout the summer growing season in California's Central Valley. This research was conducted as a part of Grape Remote sensing Atmospheric Profile & Evapotranspiration eXperiment (GRAPEX), a multi-agency effort headed by the USDA with the aim of combining in-situ and remotely-sensed data to investigate the effects of canopy structure and row orientation on light and moisture exchange processes within and above the vine canopy (Kustas *et al.*, 2018). This interdisciplinary effort has allowed for me to interact with knowledgeable experts in viticulture, biometeorology, and plant physiology – all of whom have been essential for our success in carrying out field work and subsequent data analyses. As a member of the Plant OPTICS Lab at UC Davis, our group's effort in GRAPEX has focused on monitoring vineyard physiological status and function at the canopy

scale from tower- and canopy-based remote sensing platforms. For this thesis – I will outline the theoretical basis of the work, goals and objectives, site design, methodologies, data results, and an overall discussion highlighting the lessons learned and future implications of the research.

Introduction

Responsible for providing a variety of ecosystem services, plants are essential for the facilitation of carbon sequestration from Earth's atmosphere. Plants assimilate carbon dioxide and absorb solar energy to perform photosynthesis, and the rate at which this process occurs is known as gross primary productivity (GPP). In remote sensing of the environment, empirical estimates of GPP have shown strong linear correlations with solar-induced chlorophyll fluorescence (SIF), a proxy for estimating plant photosynthetic activity (Frankenberg *et al.*, 2011). Both useful for monitoring the fate of energy in photosynthetic processes to inform changes in the global carbon cycle, GPP and SIF have shown immense potential for detecting physiological stress and seasonality (Magney *et al.*, 2017, 2019; Turner *et al.*, 2020). The quantification of GPP, SIF, and spectral-based vegetation indices presents enormous potential for real-time stress detection in plants.

Photosynthesis is a primary driver of the global carbon cycle; thus, the regulation of light energy reaching chlorophyll molecules serves as an important indicator for environmental stress detection. As light energy is absorbed by chlorophyll molecules, the molecules transition from a grounded to an excited state with three primary fates of energy: photochemical quenching (PQ), non-photochemical quenching (NPQ), and chlorophyll fluorescence (ChlF) (Baker, 2008). PQ initiates the energy transport of photons from light to photochemical reaction centers to be used for photosynthesis. The remaining light energy absorbed through chlorophyll either dissipates from the leaf as heat (i.e., NPQ) or is reemitted as light at longer wavelengths in the red and far-red regions (i.e., ChlF). Because the energy balance of light is partitioned between PQ, NPQ and ChlF, an increased efficiency for one results in a change in the other two, but it is non-linear (Butler, 2003; Porcar-Castell *et al.*, 2014b). Hence, by measuring the yield of ChlF, information

about changes in the efficiency of PQ and NPQ can be gained (Maxwell & Johnson, 2000; Magney *et al.*, 2017). Through observing how each of the three pathways respond to variations in light energy, researchers can better understand plant dynamics and their interactions within a given environment (Porcar-Castell *et al.*, 2021). Thus, understanding how plants utilize absorbed energy from light provides insight into plant function across spatial and temporal scales (Magney *et al.*, 2020).

H istorically, research linking ChlF and photosynthetic processes has been achieved through pulse-amplitude modulation (PAM) fluorometry, an active approach to interpret PQ and NPQ (Papageorgiou, 2004). ChlF has proven to be relatively easy to capture at the leaf scale in laboratory settings (Hák *et al.*, 1990; Magney *et al.*, 2017; Rajewicz *et al.*, 2019), and the ability to control light energy intensities through PAM techniques have proven to be a major strength of active approaches for measuring ChlF (Baker, 2008). Although measuring ChlF through PAM instruments allows for repeatability and controlled light modulation, such "active" approaches for measuring ChlF through PAM have inherent limitations for field-based applications due to their intensive personnel demands and upscaling restrictions. These scaling limitations have inspired alternative methodologies for measuring ChlF outside of laboratory settings.

Traditional remote sensing techniques for tracking plant phenology in field settings have been primarily based on the amount of incoming solar radiation reflected by the vegetation layer upon incidence (Zeng *et al.*, 2022). In this traditional sense, data retrieved from ground-based and remotely-sensed vegetation reflectance have provided information on chlorophyll content and plant structure. Such indices include the normalized difference vegetation index (NDVI; Tucker, 1979), enhanced vegetation index (EVI; Huete *et al.*, 2002), near-infrared reflectance of vegetation index (NIRv; Badgley *et al.*, 2017), photochemical reflectance index (PRI; Gamon *et*

al. 1992), and chlorophyll carotenoid index (CCI; Gamon *et al.*, 2016). NDVI is a greenness index that is generally used to discern vegetation from other detectable objects (eg. soil, mulch, concrete) (Pettorelli *et al.*, 2005). NDVI has also been used as a proxy for leaf area index (LAI) and fraction of absorbed photosynthetically active radiation (fAPAR) (Myneni & Williams, 1994; Knyazikhin *et al.*, 1998). Like NDVI, EVI is a greenness index; however, EVI attempts to correct for atmospheric conditions and canopy background noise particularly in areas with dense vegetation (Huete *et al.*, 2002). NIRv is the product of near-infrared reflectance and NDVI which amplifies the sensitivity of the NIR signal and has greater sensitivity (avoiding saturation) to total green leaf area, and limits the influence of background noise (Badgley *et al.*, 2017). PRI is sensitive to short-term changes in xanthophyll cycle and often used as a proxy of photosynthetic efficiency (Gamon *et al.*, 1997; Peñuelas *et al.*, 1995; Wong & Gamon, 2015a,b; Wong *et al.*, 2022). CCI tracks changes in longer term changes in carotenoid/chlorophyll pigment ratios and photosynthetic activity (Gamon *et al.*, 2016). These reflectance-based indices have been used in previous studies as indicators of photosynthetic phenology, such as GPP, in various applications and scales (Zeng *et al.*, 2022).

Because photosynthetic processes are actively regulated by plants, their efficiencies are highly variable as leaves adjust to environmental conditions (Maxwell & Johnson, 2000). Thus, it is questionable if reflectance-based methods provide sufficient detail for researchers to interpret these photosynthetic efficiencies and tradeoffs between the three pathways as light interacts with chlorophyll (Porcar-Castell *et al.*, 2021). Recent advances in technologies and methodologies have shown promise for capturing in-situ ChlF characteristics of plant systems through solar-induced chlorophyll fluorescence (SIF) (Mohammed *et al.*, 2019). SIF has broadened the potential to observe rapid changes in plant function on a variety of spatiotemporal

scales with remote sensing (Yang *et al.*, 2015; Magney *et al.*, 2019; Mohammed *et al*., 2019) and leaf-scale continuous fluorescence platforms (Porcar-Castell, 2011). Also referred to as passive ChlF, SIF has gained momentum in optical remote sensing research through correlations with GPP (Frankenberg *et al.*, 2011; Porcar-Castell *et al.*, 2014a; Sun *et al*., 2017) and has gained significant attention in general for its applicability towards broader topics in agriculture . SIF can be measured from ground-based (eg. canopy- and tower-mounted) and remotely-sensed (eg. airborne and satellite) platforms using the Fraunhofer Line Depth/Discriminator (FLD) algorithm, which estimates SIF by 'in-filling' narrow dark-lines (the Fraunhofer lines) of the electromagnetic spectrum resulting from molecular light absorption in the photosphere (Meroni *et al.*, 2009; Guanter *et al.*, 2013; Frankenberg & Berry, 2017). To scale measurements from leaf to canopy and from seconds to months, SIF, like PAM, measures radiative loss of energy of absorbed photons by chlorophyll in the red to far-red range under natural sunlight in discrete retrieval windows (Meroni *et al.*, 2009). Although the direct link between active (eg. PAM) and passive (eg. SIF) ChlF and their relationships to carbon uptake via photosynthesis remain unclear, the responsiveness of SIF to changes in the photosynthetic processes highlights its potential advantage over reflectance-based vegetation indices for its ability to predict GPP (Porcar-Castell *et al.*, 2014a).

However, current limitations exist for the passive retrieval of SIF when compared to active retrieval of fluorescence through PAM. While PAM is advantageous for measuring broadly throughout the red and far-red regions (though, mostly greater than 700 nm), remote sensing measurements are made across individual wavelengths and difficult to characterize due to its highly dynamic nature. The SIF signal is also quite weak (<5% of reflected light) when compared to leaf reflectivity observed in the red to far-red regions (Meroni *et al.*, 2009). Also, up

to 90 percent of red fluorescence photons can be re-absorbed by the leaf due to the inherent properties of overlapping absorption and emission spectra (Gitelson *et al.*, 1998). Lastly, obtaining SIF information at fine spectral, spatial, and temporal resolution under natural sunlight can be expensive, typically requiring robust operation and maintenance demands. In particular, SIF retrieval is prone to systematic and statistical errors due to dark current corrections, detector offset and nonlinearities, and stray light in the spectrometers (Grossmann *et al.*, 2018a). Along with uncertainties posed by radiometric calibration, SIF retrieval requires data quality assurance to detect and limit potential errors (Chang *et al.*, 2020).

Considering these limitations of traditional SIF retrieval, this study aims to explore an alternative approach to capture ChlF during nighttime conditions using low-cost (monetary and operational) light-emitting diodes (LEDs) lighting and photodiode/spectral sensors at the canopy-level in grape vineyards. This approach (LED-induced fluorescence, or LEDIF) was introduced to effectively measure steady-state ChlF during nighttime conditions without interference from confounding variables (i.e. solar radiation) that make retrieval difficult in normal daytime conditions (Atherton *et al.*, 2019; Romero *et al.*, 2021). LEDIF is a relatively new approach to measure ChlF and has gained traction for its applicability at leaf and canopy levels. Atherton *et al*. (2019) utilized a high-powered multispectral LED array to illuminate canopies at night, and Romero *et al.* (2021) assessed changes in soybean irrigation treatments through actively measuring LEDIF.

We constructed a canopy-based LEDIF system prototype and tested its feasibility by conducting an experiment in April 2020 to capture the impacts of drought on *P. myrtifolia* (Brissette *et al.*, *in prep*). The experiment demonstrated that the LEDIF system prototype was successful in capturing a decrease in fluorescence during the induced-drought period, followed

by an immediate recovery afterwards. The success of Brissette *et al*. (*in prep*) in creating a low-cost LEDIF system capable of detecting drought stress and recovery inspired this study's efforts by measuring LEDIF dynamics over an entire summer growing season in a drought-prone environment. Through the deployment of instruments capable of measuring canopy reflectance and fluorescence during both daytime and nighttime conditions, this study aims to compare spectral-based results (eg. vegetation indices, SIF, LEDIF) along with GPP and other meteorological parameters. The objectives of this study were to; (a) determine the feasibility of implementing an affordable, user-friendly ground-based remote sensing tool capable of capturing chlorophyll fluorescence properties within grape vineyard canopies through the implementation of blue LEDs and low-cost sensors at night, and (b) compare its results with other spectral and meteorological parameters indicative of plant physiological characteristics.

Methods

Study site

This study was conducted at a commercial grape vineyard block in California's Central Valley as part of the USDA-ARS Grape Remote Sensing Atmospheric Profile and Evapotranspiration eXperiment (GRAPEX) (Kustas *et al.*, 2018). The vineyard block was planted with merlot (*Vitis vinifera L.)* in 2010 and trained on a split trellis with a variable rate drip irrigation system that allows for delivery of irrigation amounts to vary at 30 m resolution. The block (named Ripperdan 720 located near the City of Madera, CA, USA) was divided into four subplots, each approximately 4 hectares in size: northwest (rip1), northeast (rip2), southwest (rip3), and southeast (rip4). Soil type is classified as loam/sandy loam. The vineyard subplots have east-west row orientation with 3.35 m of space between rows, approximately 1.5 m of space between vines, and maximum canopy heights ranging from 1.5 to 2.2 m. An intensive observational period (IOP) was conducted from July 29 to August 4 where two of the four subplots (rip2 and rip4) underwent different irrigation plans to actuate drought stress while the other two (rip1 and rip3) remained consistent with usual irrigation. While the two control subplots (rip1 and rip3) underwent typical, drip irrigation throughout the IOP, the drought-stressed subplots (rip2 and rip4) were restricted from access to water via irrigation altogether. It should be noted that there was no water in the form of precipitation during the IOP.

Tower-based SIF system

A tower-based spectrometer system was located central to the four vineyard subplots (*Figure 1a*). Also known as PhenoSpec (Wong *et al*., 2022, *in review*), the tower-based system was modified from the PhotoSpec system described in Grossmann *et al.* (2018) consisting of a two-dimensional scanning telescope unit mounted at a height of 12 m for repeat targeted views.

The tower-based spectrometer system operated diurnally, thus allowing for passive spectral measurements to be made when solar radiation was present during daytime conditions. Canopy spectra were determined using both Flame VIS-NIR and QE Pro spectrometers (Ocean Insight, Florida, USA). The Flame VIS-NIR (hereafter referred to as, Flame) spectrometer operates with a 350 to 1000 nm wavelength range and 1.33 nm full width half maximum (FWHM) optical resolution. The QE Pro spectrometer operates with a 730 to 780 nm wavelength range and narrowed 0.3 nm FWHM optical resolution (*Figure 1b*).

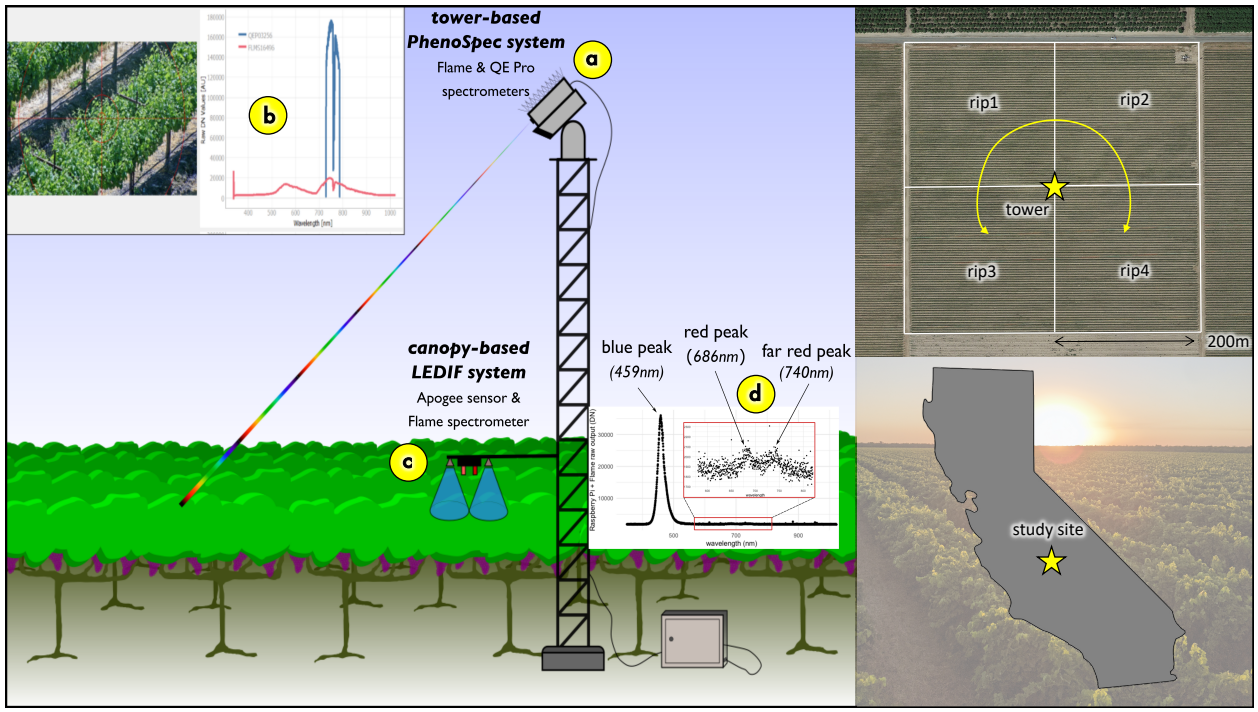

Figure 1: General schematic of tower-based PhenoSpec (a,b) and canopy-based LEDIF (c,d) systems. The systems were located at a Merlot grape vineyard study site in Madera, California and were fixed to a tower structure centrally located between four subplots: rip1 (NW), rip2 (NE), rip3 (SW), and rip4 (SE).

Six target locations were randomly selected for each vineyard subplot. Of the six targets, three were selected at near proximity to the tower (within 30 m of the tower's base), and the other three were located further away (between 30 and 100 m from the tower's base). The camera continuously rotated between subplots rip1 through rip4 (in order of rip3, rip1, rip2, rip4) every three targets, capturing spectra from each target at near proximity before repeating the

process for the targets further from the tower. An upward-facing sky measurement was captured every six targets, or between every two subplots. Sky-facing measurements, known as irradiance, were captured through an opal lens diffuser with 30 percent transmission efficiency, which were later used to quantify radiance (Wong *et al*., *in review*). Target and sky measurements occurred with integration time being automatically adjusted to optimize for signal-to-noise and prevent saturation due to incoming solar radiation (at 80% signal saturation). A full cycle across all subplots (six targets per plot; $n_{target} = 24$, $n_{sky} = 8$) took about 60 minutes, and a semi-plot cycle (three targets per plot; $n_{target} = 12$, $n_{sky} = 4$) took about 30 minutes. While ultimately depending on signal saturation from solar radiation, on average, one measurement was captured for every two minutes.

Data processing and normalization

Raw spectral data output from the Flame and QE Pro spectrometers required radiometric calibration to convert from digital numbers (DN) to radiance (W cm^{-2} sr^{-1} nm^{-1}). First, a pre-calibrated full-range spectroradiometer, SVC HR-1024i (Spectral Vista Corporation, New York, USA), is pointed at white reference panel to capture radiance every minute for 90 minutes capturing wavelengths between 350 and 2500 nm during midday, under full sun. Pointed at the same white reference panel, the PhenoSpec spectrometers also collected spectra using the same measuring frequency (every minute for 90 minutes), thus resulting in 90 measurements for each instrument as well. Then, a linear fit between the PhenoSpec spectrometers and SVC allows for the direct calibration measurement linkage between the digital numbers and radiance, respectively. With linear fits extracted for each measurement, calibration coefficients are extracted as the slope values for each wavelength. Radiance values for the PhenoSpec

spectrometers are then quantified as the product of raw output data (digital numbers) and the extracted calibration coefficients.

The radiometric calibration process to obtain radiance for both spectrometers can be visualized in *Supplemental Figure 1* and is described in full detail by Wong *et al*. (*in review*). Reflectance was then calculated for each target measurement by dividing radiance by the corresponding sky measurement nearest in time for both the Flame and QE Pro spectrometers. The following vegetation indices were calculated from the tower-based Flame spectral data: normalized difference vegetation index (NDVI), enhanced vegetation index (EVI), near-infrared reflectance of vegetation index (NIRv). photochemical reflectance index (PRI), and chlorophyll carotenoid index (CCI). NDVI was calculated as $NDVI = (R_{NIR} – R_{Red}) / (R_{NIR} + R_{Red})$, where R_{NIR} is the average reflectance from 830 to 860 nm and R_{Red} is the average reflectance from 620 to 670 nm. EVI was calculated as $EVI = (R_{758} – R_{670}) / (R_{758} + (6 * R_{670}) – (7.5 * R_{470}) + 1)$, where R_{758} is the average reflectance from 753 to 763 nm, R_{670} is the average reflectance from 665 to 675 nm, and R_{470} is the average reflectance from 465 to 475 nm. NIRv was calculated as $NIRv = NDVI * R_{NIR}$. PRI was calculated as $PRI = (R_{531} – R_{570}) / (R_{531} + R_{570})$, where R_{531} is the average reflectance from 526 to 536 nm and R_{570} is the average reflectance from 565 to 575 nm. CCI was calculated as $CCI = (R_{531} – R_{645}) / (R_{531} + R_{645})$, where R_{531} is the average reflectance from 526 to 536 nm and R_{645} is the average reflectance from 640 to 650 nm. SIF retrieval was conducted through the Fraunhofer Line Depth (FLD) method by infilling the atmospheric O_2~A absorption feature (Meroni et al., 2009). SIF was then quantified using a combination of spectral radiance (L) and irradiance (E) at 757.5 ($\lambda_{757.5}$) and 760.5 ($\lambda_{760.5}$). SIF was calculated as $SIF = ((E_{757.5} * L_{760.5}) – (L_{757.5} * E_{760.5})) / (L_{760.5} – E_{760.5})$. Relative SIF was calculated as $SIFravg = SIF / L_{760.5}$, and its product is useful for normalizing SIF by reflected radiance to account for

variability in incoming irradiance and bidirectional reflectance effects (Magney *et al.*, 2019). All indices/products and their respective formulas listed above are shown in *Table 1*. Vegetation indices and SIF measurements were then averaged by target and per plot to the nearest half hourly window to match the half hourly eddy covariance measurements. Daily means were calculated from 11:00 to 16:00 (time window used to avoid angular impacts) for tower-based spectrometers (NDVI, EVI, NIRv, PRI, CCI, SIF, and SIFravg) and eddy covariance data. It should be noted that all SIF values are calculated daily means from individual SIF measurements greater than -0.025 and less than 0.075. For all PhenoSpec data, a threshold was implemented at NDVI = 0.3 to exclude non-vegetation points. Because NDVI indicates greenness reflected from vegetation, targets captured with reflectance below this threshold were identified and excluded from daily means and subsequent steps in analyses. *Supplemental Figure 2* demonstrates NDVI histograms for all target measurements and those above the threshold. Five-day running means were used to smooth the timeseries data.

Table 1: PhenoSpec data products and indices

tower-based PhenoSpec system: indices/products and their formulas	
Index/Products	Formula
NDVI	$(R_{NIR} - R_{Red}) / (R_{NIR} + R_{Red})$
EVI	$(R_{758} - R_{670}) / (R_{758} + (6 * R_{670}) - (7.5 * R_{470}) + 1)$
NIRv	$NDVI * R_{NIR}$
PRI	$(R_{531} - R_{570}) / (R_{531} + R_{570})$
CCI	$(R_{531} - R_{645}) / (R_{531} + R_{645})$
SIF	$((E_{757.5} * L_{760.5}) - (L_{757.5} * E_{760.5})) / (L_{760.5} - E_{760.5})$
SIFravg	$SIF / L_{760.5}$

Eddy Covariance

Micrometeorological and carbon flux measurements were collected for the full growing season using eddy covariance flux towers located in the southeast corner of each subplot, where each tower was equipped with identical instrumentation. The flux tower systems were each equipped with an integrated open path infrared gas analyzer and sonic anemometer, IRGASON (Campbell Scientific Inc., Utah, USA) mounted 4.5 m above local ground level facing west. Fluxes were collected at 20 Hz and surface fluxes were estimated over 30 min time periods. Anomalous records in the high-frequency data were removed by using a de-spiking moving window algorithm. Flux estimates were corrected by applying a two-dimensional coordinate rotation of the three wind speed components, as well as for sensor displacement and frequency response attenuation. Sonic temperatures were corrected based on (Schotanus *et al.*, 1983), and the resulting fluxes were adjusted by the Webb, Pearman and Leuning (WPL) density corrections (Webb *et al.*, 1980). Additional meteorological instruments consisted of a NR01 net radiometer (Hukseflux, Netherlands), an EE08 temperature and relative humidity probe (E+E Elektronik, Austria) in an aspirated shield (Apogee Instruments, Utah, USA), and a soil moisture and temperature sensor (Stevens HydraProbe, Oregon, USA) installed at 5 cm depth (only soil temperature used). Results from the eddy covariance system used in this study include: air temperature, soil temperature, relative humidity, solar radiation, net radiation, water vapor pressure, ambient air pressure, vapor pressure deficit, gross primary productivity, ecosystem respiration, latent heat flux, sensible heat flux, and wind speed.

Canopy-based LEDIF system

A canopy-based LEDIF system (*Figure 1c*) was also positioned at the base of the PhenoSpec tower for the duration of the study period, from July through October 2021. The

canopy-based system was mounted in a fixed position 2.4 m above local ground level, extending 1.8 m perpendicular from the tower, and 0.2 to 0.9 m above the maximum canopy height. The variation in maximum canopy height resulted from the grapevines growing towards the fixed canopy-based system as the growing season progressed. The canopy-based system consisted of an Apogee PAR photodiode sensor (Apogee Instruments, Utah, USA), an Apogee Red/Far-Red photodiode sensor, a Flame VIS-NIR spectrometer (Ocean Insight, Florida, USA) operated through a Raspberry Pi 4 computer, and five LEDs (two at 15 W and three at 5 W). The Apogee PAR sensor operates with a spectral range of 400-700 nm, and the Apogee Red/Far-Red sensor is sensitive to 645-665 nm and 720-740 nm for the red and far-red regions, respectively. The LEDs emitted light only in the blue region of the spectrum; therefore, any spectral response in the red/far-red regions could safely be regarded as a ChlF response as the reemission of blue light (*Figure 1d*). The Flame spectrometer captured spectra at a one minute interval between the hours of 10:00-15:00 (daytime) and 23:00-01:00 (nighttime). The Apogee PAR and Red/Far-Red sensors captured measurements every five minutes, 24 hours per day. While daytime measurements were taken by all instruments in the LEDIF system, non-nighttime measurements were not considered, and thus, omitted from further investigation in this study.

The intensity of light emitted from the LEDs were conducted in the lab prior to the system's deployment at the study site with the intent to ensure its signal could be detected from a reasonable distance. Over the duration of the study period, the LED lights were activated for 30 minutes between the hours of 00:00 and 00:30. At the study site, the Apogee sensors, fiber optic cable connected to the Flame spectrometer, and LED lights were positioned directly above and oriented downwards facing towards the grapevine canopy. The canopy-based LEDIF system was designed to consistently capture spectra in a smaller spatial area consistently throughout the

study with a field of view at roughly 1.34 nm FWHM. *Figure 2* shows a top-down perspective of the LEDIF setup from just above the grapevine canopy and provides visual context for the various components and orientation of the study site and system design.

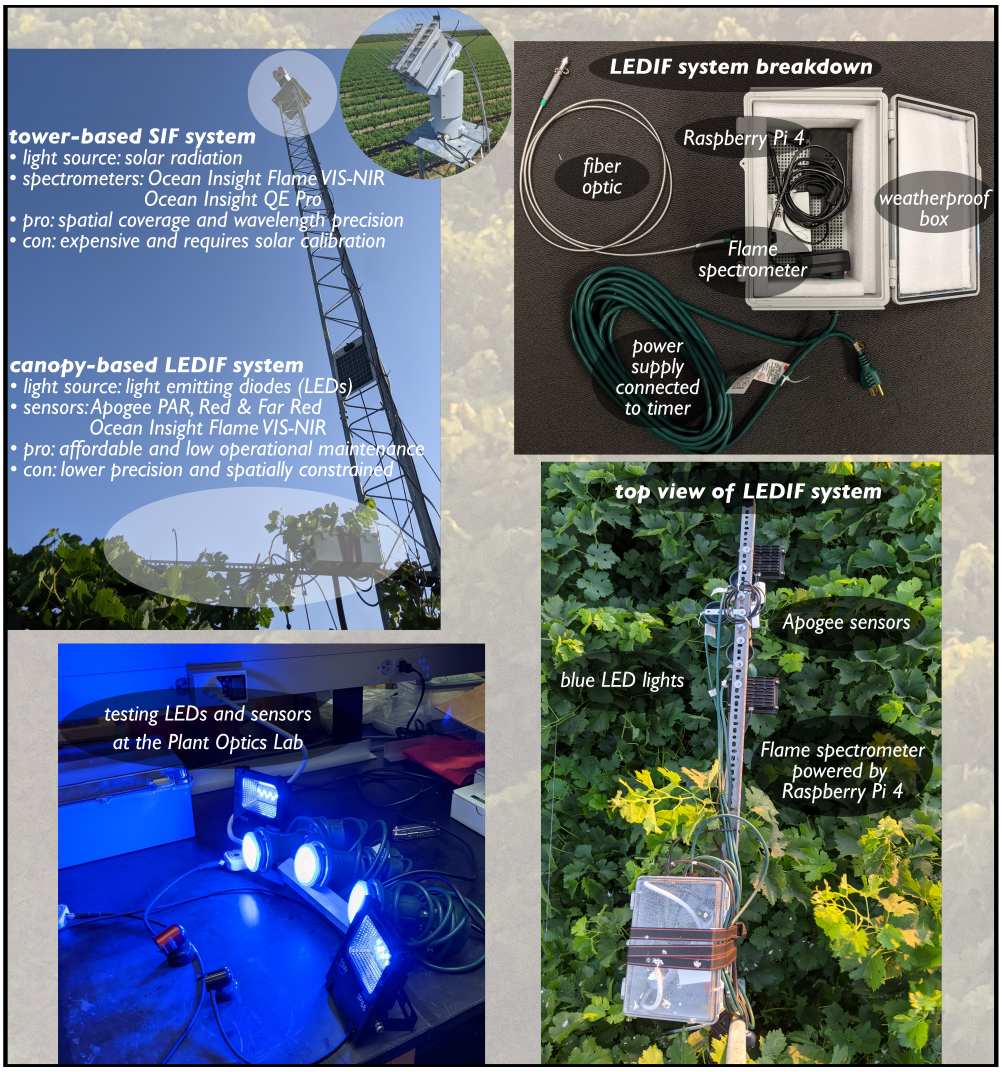

Figure 2: Photos and descriptions of both tower-based PhenoSpec and canopy-based LEDIF systems. Top-down perspective of the LEDIF setup from just above the grapevine canopy and provides visual context for the study site and system design.

Data processing and normalization

While radiometric calibration is necessary for spectrometers operating in daytime conditions to obtain radiance from digital numbers, this process is only made possible through the comparison of raw output spectra with spectra captured through a white reference panel

spectra in summer, clear daytime conditions. Because of its operation during nighttime conditions, the LEDIF system raw output measurements from both the Apogee Red/Far-Red sensor (μmol * m-2 * s-1) and Flame spectrometer (Digital Numbers) required further normalization to account for the varying scales and distributions of such data. As a result, various approaches of data normalization were considered due to the grapevine encroachment on the system throughout the study period. The first normalization approach involves the utilization of blue region (400-500 nm) spectra to normalize raw outputs captured in the red and far-red regions. Due to their varying wavelength constraints and output formats, visible light-based normalization was conducted differently for the Apogee sensor and Flame spectrometer. Since the Flame captures spectra continuously throughout the visible and NIR regions, its broad range allowed for more options in the normalization of nighttime data. Because the LED lights emitted lights solely in the blue region, its spectra consistently demonstrated a normal distribution with a notable peak roughly around 460 nm (*Figure 1d*). The full-width at half maximum (FWHM) of this blue peak could then be identified and for each measurement taken by the sensor throughout the study period. By averaging the raw output values within the FWHM range at each measurement, mean intensities of this blue region peak were then used as a denominator to normalize spectra captured in the red and far-red regions. Because the Apogee Red/Far-Red sensor outputs in non-wavelength format, rather simply as “Red” and “Far-Red”, wavelength-specific normalization was not an option. Due to this constraint, output measurements from the Apogee Red/Far-Red sensor were normalized by respective measurements taken by the Apogee PAR sensor (400-700nm). As with the Flame, any radiation captured by the Apogee PAR sensor can confidently be attributed to the blue region due to the LED lights being the only source of light.

The second approach to normalize raw output measurements in red and far-red spectra consisted of utilizing minimum and maximum values for each wavelength. Known as unity-based normalization, this technique was selected because of its consistency for both the Flame spectrometer and Apogee Red/Far-Red sensor. Because unity-based normalization can be applied to both discrete and continuous wavelength regions, the formula to normalize remains the same for both instruments in the LEDIF system. Normalized intensities (i_{norm}) for all data captured through the unity-based approach were calculated using the following expression: $i_{norm} = (i - i_{minimum}) / (i_{maximum} - i_{minimum})$. *Table 2* highlights instrument specifications for both the tower-based Phenospec and canopy-based LEDIF system, including details on sampling intervals, wavelength ranges, data types, units, and calibration/normalization performed in this study. To expand on the normalization details listed in *Table 2*, *Table 3* outlines computational details for blue region- and unity-based normalization of raw output data from the Flame spectrometer and Apogee Red/Far-Red sensor.

Table 2: Instrument specifications distinguished by sampling conditions and system type.

tower-based PhenoSpec system: *instrument specifications (daytime conditions)*

Spectrometer/Sensor	Sampling Period (2021/07/19 – 2021/10/01)	Wavelength Range	Raw Output Units	Calibration/Normalization Performed	Units after Calibration	Yielding results
Ocean Insight Visible-NIR Flame Spectrometer	Continuous rotation through plot targets during daytime (6 targets per plot, 4 plots total)	350 – 1000 nm	digital numbers (DN)	radiometric calibration	radiance (W * cm-2 * nm-1* sr-1)	Reflectance, NDVI, PRI, CCI, EVI, NIRv
Ocean Insight QE Pro Spectrometer	Continuous rotation through plot targets during daytime (6 targets per plot, 4 plots total)	730 – 780 nm	digital numbers (DN)	radiometric calibration	radiance (W * cm-2 * nm-1* sr-1)	SIF

canopy-based LEDIF system: *instrument specifications (nighttime conditions)*

Spectrometer/Sensor	Sampling Period (2021/07/19 – 2021/10/01)	Wavelength Range	Output Units	Calibration/Normalization Performed	Units after Calibration	Yielding Results
Ocean Insight Visible-NIR Flame Spectrometer	1-minute measurement interval between 10:00-15:00 and 23:00-01:00	350 – 1000 nm	digital numbers (DN)	blue region-based normalization (FWHM of LED-induced blue peak), unity-based normalization	unitless	red peak, far-red peak (LEDIF), red/far-red ratio
Apogee Red/Far-Red Sensor	5-minute measurement interval for 24 hours/day	645 – 665 nm (red) 720 – 740 nm (far-red)	µmol * m-2 * s-1	blue region-based normalization (PAR), unity-based normalization	unitless	red peak, far-red peak (LEDIF), red/far-red ratio
Apogee PAR Sensor	5-minute measurement interval for 24 hours/day	400 – 700 nm	µmol * m-2 * s-1	–	–	–

Table 3: Canopy-based LEDIF system details for sensors and spectrometers. Table shows results for both instruments of raw output data (top), blue-region based normalization (middle), and unity-based normalization (bottom).

canopy-based LEDIF system: *raw output data*

Result	Raspberry Pi + Flame	Units	Apogee Red-Far Red	Units
Red Peak	$Intensity_{686}$ (LED mean) / $Intensity_{686}$ (Dark mean)	DN / DN	Red (LED mean) / Red (Dark mean)	µmol * m-2 * s-1 / µmol * m-2 * s-1
Far-Red Peak (LEDIF)	$Intensity_{740}$ (LED mean) / $Intensity_{740}$ (Dark mean)	DN / DN	Far-Red (LED mean) / Far-Red (Dark mean)	µmol * m-2 * s-1 / µmol * m-2 * s-1
Red / Far-Red Ratio	Red Peak / Far Red Peak	*unitless*	Red Peak / Far-Red Peak	*unitless*

canopy-based LEDIF system: *blue region-based normalization*
Apogee – normalize by photosynthetically-active radiation (PAR) sensor
Raspberry Pi + Flame – normalize red/far-red intensities by FWHM of LED-induced blue peak

Result	Raspberry Pi + Flame	Units	Apogee Red-Far Red	Units
Red Peak	$Intensity_{686}$ (i_{LED}) – $Intensity_{FWHM}$ (i_{LED}) / $Intensity_{686}$ (i_{Dark}) – $Intensity_{FWHM}$ (i_{Dark})	DN / DN	Red (i_{LED}) – PAR (i_{LED}) / Red (i_{Dark}) – PAR (i_{Dark})	(µmol * m-2 * s-1) / (µmol * m-2 * s-1)
Far-Red Peak (LEDIF)	$Intensity_{740}$ (i_{LED}) – $Intensity_{FWHM}$ (i_{LED}) / $Intensity_{740}$ (i_{Dark}) – $Intensity_{FWHM}$ (i_{Dark})	DN / DN	Far-Red (i_{LED}) – PAR (i_{LED}) / Far-Red (i_{Dark}) – PAR (i_{Dark})	(µmol * m-2 * s-1) / (µmol * m-2 * s-1)
Red / Far-Red Ratio	Red Peak / Far-Red Peak	*unitless*	Red Peak / Far-Red Peak	*unitless*

canopy-based LEDIF system: *unity-based normalization*
Apogee & Raspberry Pi + Flame: normalize red/far-red intensities by respective minimum and maximum values

Result	Raspberry Pi + Flame	Units	Apogee Red-Far Red	Units
Red Peak	$Intensity_{686}$ (i_{LED} – min(i_{LED}) / max(i_{LED}) – min(i_{LED})) / $Intensity_{686}$ (i_{Dark} – min(i_{Dark}) / max(i_{Dark}) – min(i_{Dark}))	DN / DN / DN / DN	Red (i_{LED} - min(i_{LED}) / max(i_{LED}) - min(i_{LED})) / Red (i_{Dark} - min(i_{Dark}) / max(i_{Dark}) - min(i_{Dark}))	(µmol * m-2 * s-1 / µmol * m-2 * s-1) / (µmol * m-2 * s-1 / µmol * m-2 * s-1)
Far-Red Peak (LEDIF)	$Intensity_{740}$ (i_{LED} – min(i_{LED}) / max(i_{LED}) – min(i_{LED})) / $Intensity_{740}$ (i_{Dark} – min(i_{Dark}) / max(i_{Dark}) – min(i_{Dark}))	DN / DN / DN / DN	Far-Red (i_{LED} - min(i_{LED}) / max(i_{LED}) - min(i_{LED})) / Far-Red (i_{Dark} - min(i_{Dark}) / max(i_{Dark}) - min(i_{Dark}))	(µmol * m-2 * s-1 / µmol * m-2 * s-1) / (µmol * m-2 * s-1 / µmol * m-2 * s-1)
Red / Far-Red Ratio	Red Peak /Far-Red Peak	*unitless*	Red Peak /Far-Red Peak	*unitless*

After performing normalization for all raw output data from both the Flame spectrometer and Apogee sensors, daily mean intensities were derived for each light condition (LED and dark) for the entire study period. Because the LED lights were active for 30 minutes (00:00 – 00:30) but the Flame spectrometer and Apogee sensors recorded data during nighttime conditions beyond this LED sampling window, the system was able to capture red and far-red intensities before, during, and after the activation period. To account for timing accuracy between the LED lights and the sensors/spectrometer, daily mean intensities were quantified for a ten-minute period for each light period (00:10 – 00:20 for LED, and 00:40 – 00:50 for dark) during nighttime conditions. *Figure 3* visualizes red and far-red chlorophyll responses to LED and dark light periods at nighttime conditions for both the Apogee sensor and Flame spectrometer. The increased red and far-red intensities spanning the LED period indicates there was a detectable chlorophyll response from both instruments.

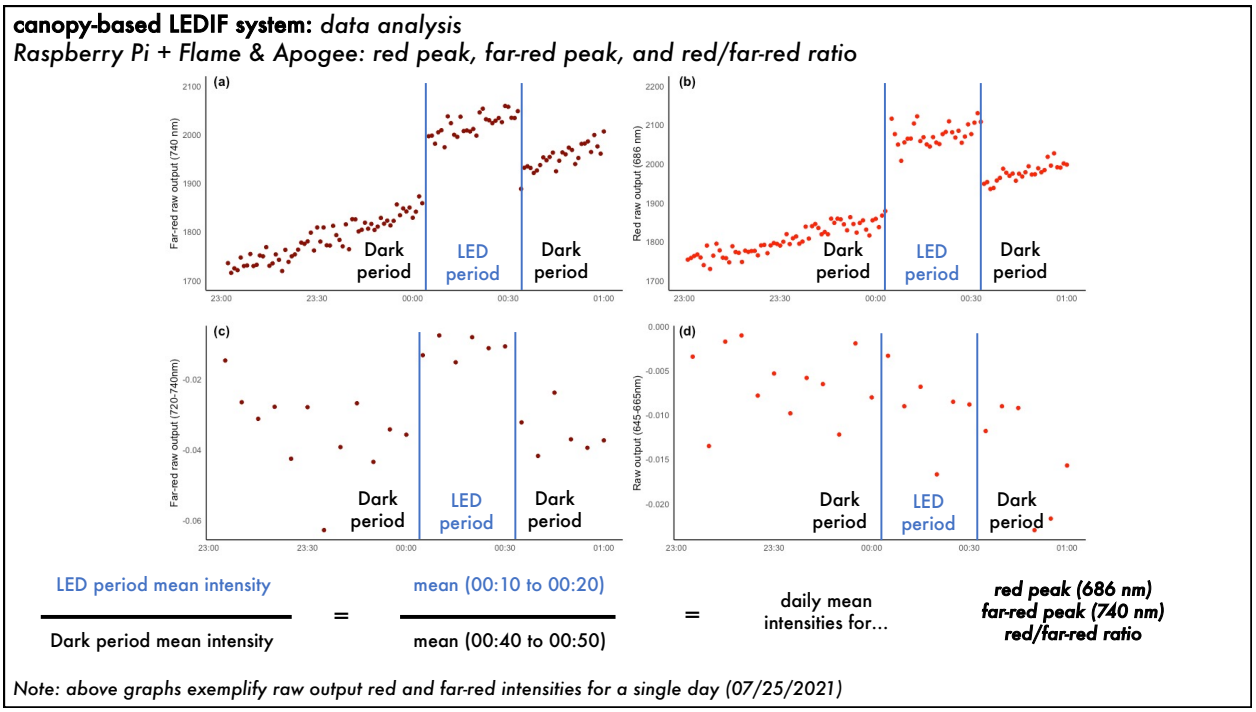

Figure 3: Raw output intensities for LED and dark periods indicating: Flame spectrometer (a) red and (b) far-red regions, as well as the Apogee sensor (c) red and (d) far-red regions.

Statistical analysis

Statistical analyses in this study were all performed in R (R Development Core Team, 2020). Variable relationships were compared using linear models to assess variance used to analyze random forest analyses were conducted to distinguish variable importance for explaining the variation of GPP during the entire and intensive observational periods events. Variables used for explaining variation of GPP are obtained from eddy covariance, meteorological, and spectral data. The randomForest package (Liaw & Wiener, 2002) was used to to run iterations with three variables randomly selected at each classification tree split until all predictor variables were stabilized.

Results

Canopy-based LEDIF system timeseries

Figure 3 shows red and far-red chlorophyll responses to LED and dark light periods during nighttime conditions for both the Apogee sensor and Flame spectrometer for a single day (July 25th) within the study period. The increased red and far-red intensities spanning the LED period (00:00 – 00:30) indicates chlorophyll fluorescence response from each of the instruments. For the Flame instrument (*Figure 3a/3b*), there is a clear spectral response in both the red and far-red regions due to the LED activation. However, while there is a discernable response from the Apogee sensor in the far-red region (*Figure 3c*), the red region response yielded higher noise and less detectability between the LED and dark periods.

Normalized daily intensities for both LED and dark periods during nighttime conditions were calculated for both the Apogee Red/Far-Red sensor and Flame spectrometer. Results for normalized daily mean intensities for each instrument are presented as red peaks, far-red peaks, and red/far-red ratios, all of which are unitless for both instruments due to the quotient between LED and dark periods. For the Flame spectrometer, the red and far-red peaks occurred at roughly 686 and 740 nm, respectively, throughout the entire study period. The red/far-red ratio was calculated as the quotient between the red peak and far-red peaks. *Figure 4* illustrates these results as a collection of timeseries for the Apogee sensor, and *Figure 5* shows the same for the Flame spectrometer. Visualized in columnar order – *Figures 4a/c/e* and *5a/c/*e show daily mean red and far-red peaks, while *Figures 4b/d/f* and *5b/d/f* show the red/far-red ratios. Visualized in row order – *Figures 4a/b* and *5a/b* show non-normalized data (raw output), *Figures 4c/d* and *5c/d* show blue region-based normalized data (FWHM for Flame, PAR for Apogee), and *Figures 4e/f* and *5e/f* show unity-based normalized data.

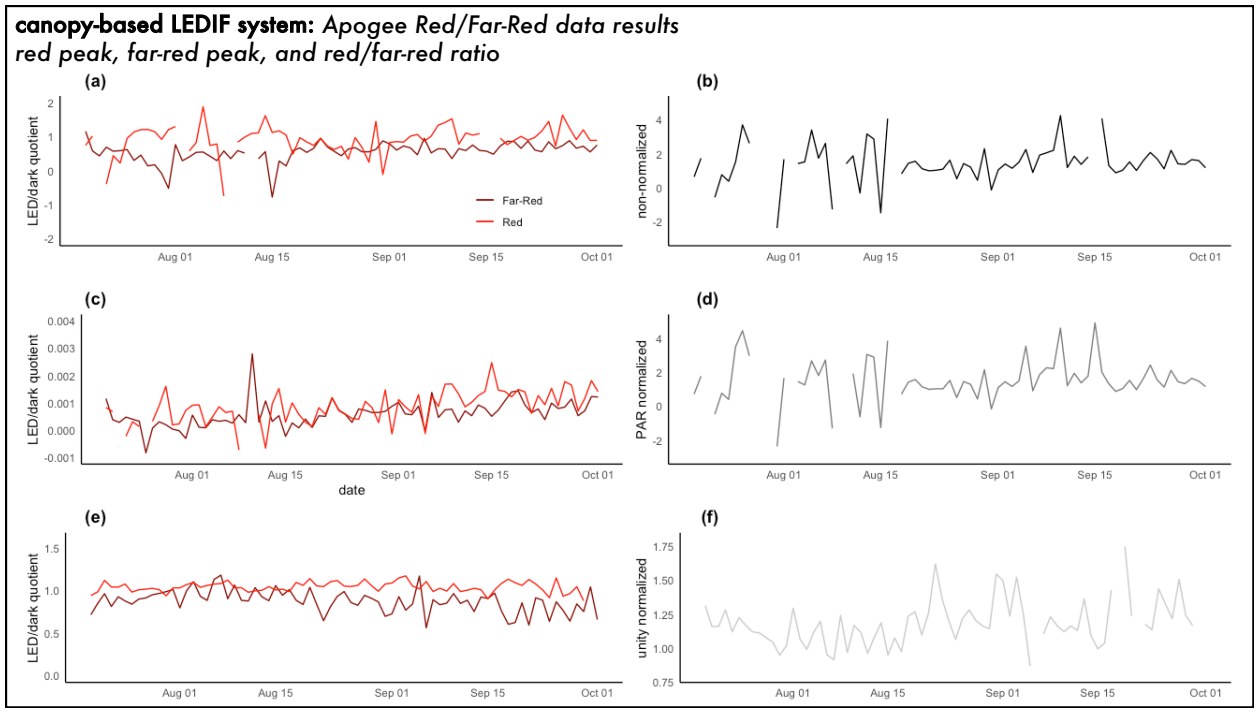

Figure 4: Apogee sensor results of red and far-red peaks, as well as red/far-red ratios for: (a,b) non-normalized, (c,d) blue-region PAR normalized, and (e,f) unity-based normalized data.

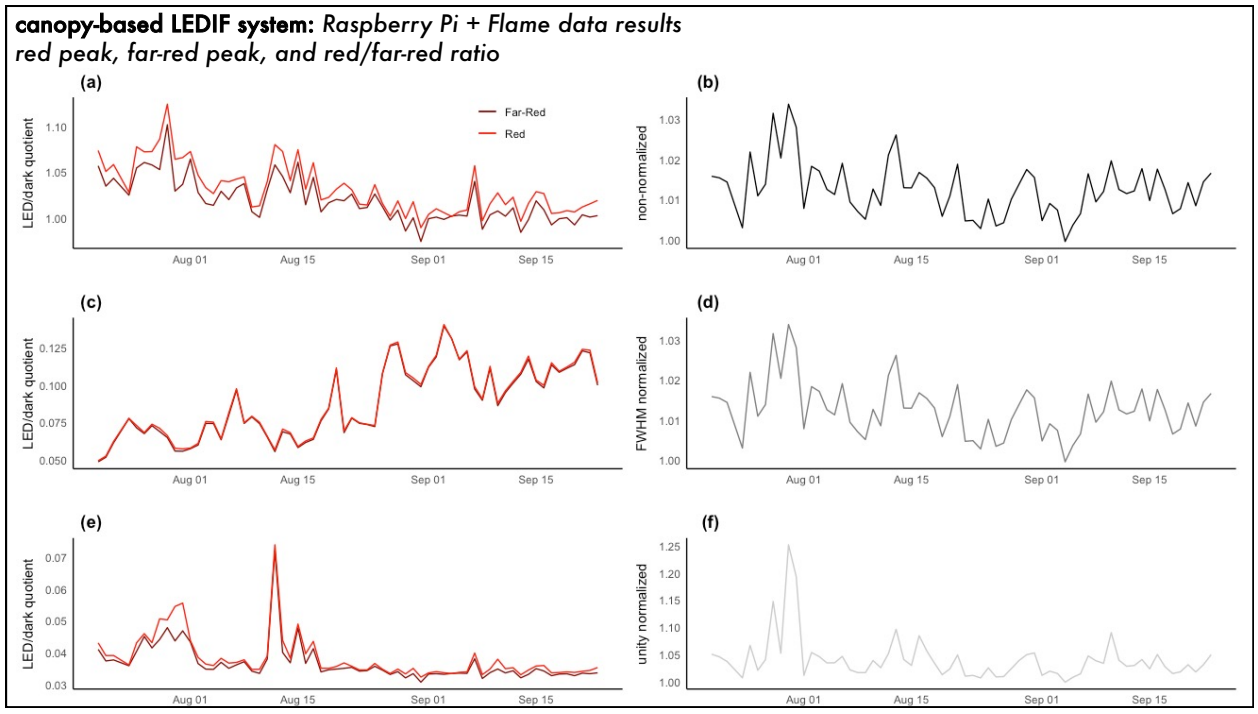

Figure 5: Flame spectrometer results of red and far-red peaks, as well as red/far-red ratios for: (a,b) non-normalized, (c,d) blue-region FWHM normalized, and (e,f) unity-based normalized data.

Given the wide range of intensities on a daily basis, normalization was necessary to accurately quantify variability in red and far-red intensities. The Apogee sensor exhibited relatively noisy red and far-red intensities for both non-normalization and blue-region based (PAR) normalization scenarios but demonstrated more consistent daily mean intensities under unity-based normalization. Conversely, red and far-red intensities for the Flame spectrometer demonstrate overall consistent trends throughout the study period for both non-normalization and unity-based normalization scenarios. However, the FWHM method showed an opposing upward trend with little differentiation between the red and far-red intensities. *Figure 5c* demonstrates this lack of differentiation between the red and far-red intensities, and *Figure 5d* exhibits the red/far-red ratio for the FWHM method as only slightly unique from the non-normalized method.

Eddy covariance

Meteorological data results are represented in *Figure 6* with the IOP highlighted as the grey band spanning from July 29th through August 4th. Air temperature remains consistent (*Figure 6a*), while soil temperature steadily declines (*Figure 6b*) throughout the study period. Relative humidity fluctuates regularly within a constant range (*Figure 6c*). Longwave and shortwave solar radiation (*Figure 6d*) along with net radiation (*Figure 6e*) demonstrate a steady decline, typical for the study period beginning in mid-summer and ends in early fall. Water vapor pressure (*Figure 6f*) and vapor pressure deficit (*Figure 6g*) both exhibit fluctuating patterns. Gross primary productivity (GPP, *Figure 6h*) remains stable for roughly the first half of the study before gradually decreasing as fall approached while ecosystem respiration (*Figure 6i*) continuously declined.

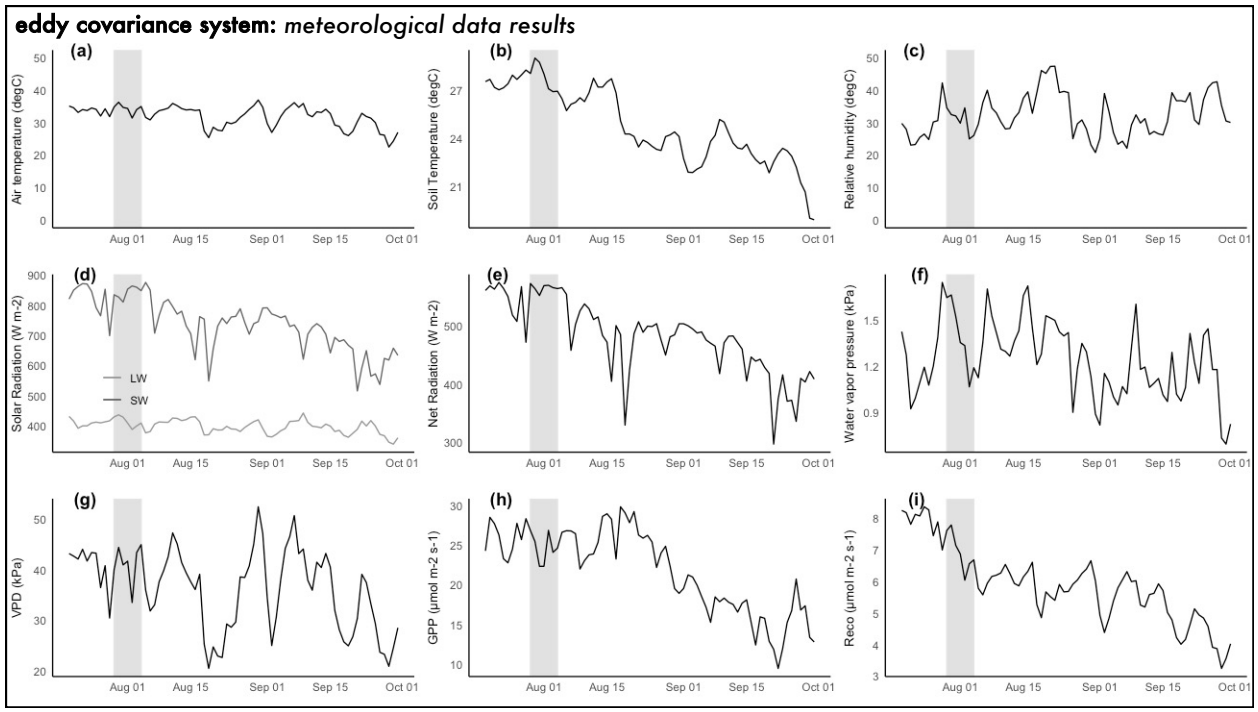

Figure 6: Meteorological data results from the eddy covariance system for the entire observational period (EOP) with the gray band highlighting the intensive observational period (IOP). Results are displayed as daily averages for (a) air temperature, (b) soil temperature, (c) relative humidity, (d) shortwave and longwave solar radiation, (e) net radiation, (f) water vapor pressure, (g) vapor pressure deficit, (h) gross primary productivity, and (i) ecosystem respiration.

Tower-based PhenoSpec system timeseries

Daily averages of reflectance-based vegetation indices (NDVI, NIRv, PRI, CCI, EVI) and solar-induced fluorescence (SIF) were calculated under clear, sunny daytime conditions. *Figure 7* details the individual subplots with rip2 and rip4 undergoing drought-induced stress during the IOP, while rip1 and rip3 irrigation remained constant throughout the IOP and overall EOP. The stressed (rip2 and rip4) and non-stressed (rip1 and rip3) subplots were grouped by their respective drought-stress conditions and are represented as such in *Figure 8*. Continuous measurements of NDVI (*Figures 7a/8a*) demonstrate a general decrease throughout the EOP with a temporary increased spike in mid-August for both conditions just following the IOP. NIRv (*Figures 7b/8b*) demonstrates a stable trend in general for both drought-conditions with minor variation on a daily basis. PRI (*Figures 7c/8c*) and CCI (*Figures 7d/8d*) both exhibit

downward trends spanning the study period; however, each demonstrate a rapid decline followed by an increased spike for both drought stressed and non-stressed conditions following the IOP. However, EVI (*Figures 7e/8e*) does not follow the same downward trend as NDVI, PRI, and CCI – increasing through late-August until steadily declining for the remainder of the study. SIF (*Figures 7f/8f*) exhibits an increased spike during the IOP; however, all subplots demonstrate decreasing trend throughout the duration of the study. However, SIF appears to have more of a distinguishable difference between the non-stressed and drought-stressed conditions compared to those of the reflectance-based indices. *Supplemental Figure 8* demonstrates these daily means of filtered SIF as trendlines and standard deviations as points, each grouped by day and subplot.

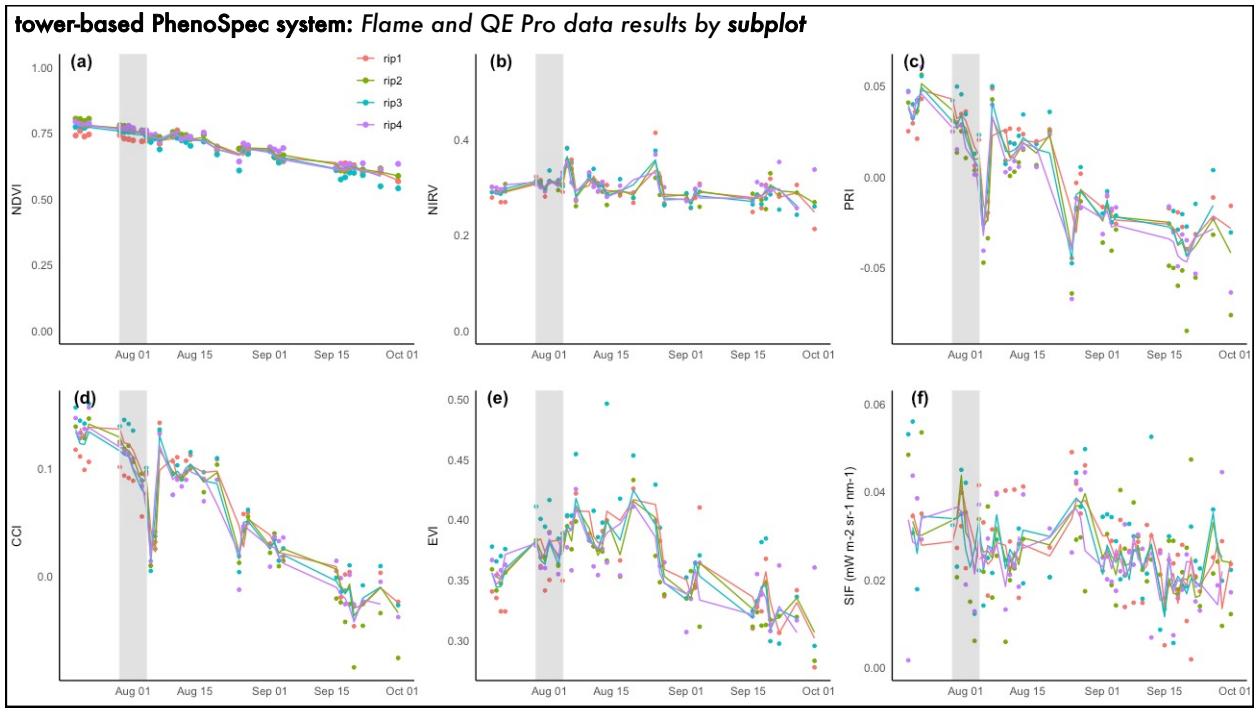

Figure 7: Tower-based PhenoSpec system results for the Flame and QE Pro spectrometers. Reflectance-based vegetation indices from the Flame spectrometer are shown as daily averages separated by subplot for (a) normalized difference vegetation index (NDVI), (b) near-infrared reflectance of vegetation index (NIRv), (c) photochemical reflectance index (PRI), (d) chlorophyll carotenoid index (CCI), and (e) enhanced vegetation index (EVI). The QE Pro spectrometer results yield (f) solar-induced fluorescence (SIF)..

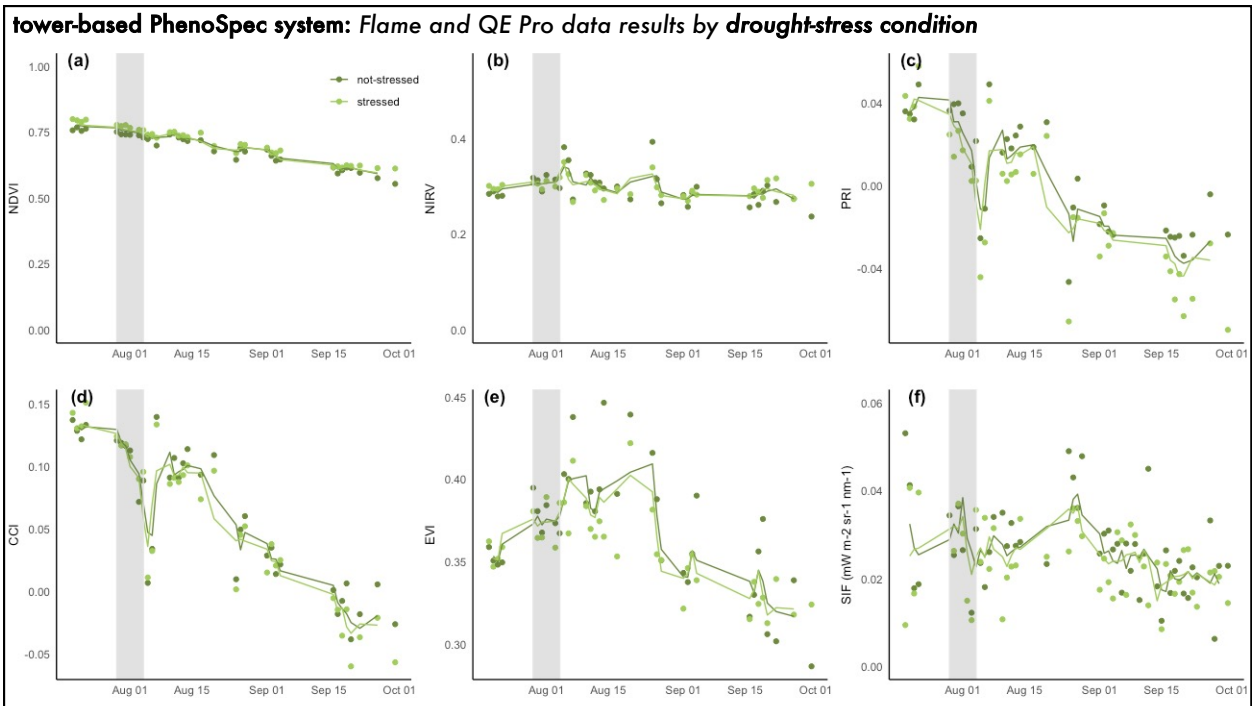

Figure 8: Similar to Figure 7; however, subplots are grouped by non-stressed and drought-stressed treatment conditions that occurred during the IOP (indicated by gray band).

Linear models for canopy-based LEDIF, tower-based PhenoSpec, and eddy covariance systems

Scatterplots of the relationships between canopy-based LEDIF unity-based normalized results from the Flame spectrometer (red peak, far-red peak, red/far-red ratio) and tower-based PhenoSpec spectrometers (vegetation indices and SIF) are shown in *Figure 9*. Linear comparisons between daytime yields averaged across all four subplots and daily nighttime averages for red peak intensities are shown in *Figure 9a/b*, far-red peak intensities are shown in *Figure 9c/d*, and red/far-red ratios are shown in *Figure 9e/f*. The explained variance for linear relationships between the nighttime canopy-based LEDIF system and daytime tower-based PhenoSpec results expressed as coefficients of determination (multiple r-squared) and p-values are as follows: red peak (NDVI = 0.21, $p < 0.001$; NIRv = 0.01, $p < 0.001$; PRI = 0.18, $p < 0.001$; CCI = 0.20, $p < 0.001$; EVI = 0.03, $p < 0.001$; SIF = 0.03, $p < 0.001$); far-red peak (NDVI = 0.17, $p < 0.001$; NIRv = 0.01, $p < 0.001$; PRI = 0.14, $p < 0.001$; CCI = 0.17, $p < 0.001$; EVI =

0.03, p < 0.001; SIF = 0.03, p < 0.001); and red/far-red ratio (NDVI = 0.13, p < 0.001; NIRv = 0.01, p = 0.005; PRI = 0.12, p < 0.001; CCI = 0.12, p < 0.001; EVI = 0.05, p = 0.05; SIF = 0.02, p < 0.001). Overall, the nighttime results from the LEDIF system do not demonstrate strong linear correlations with daytime results from the PhenoSpec system.

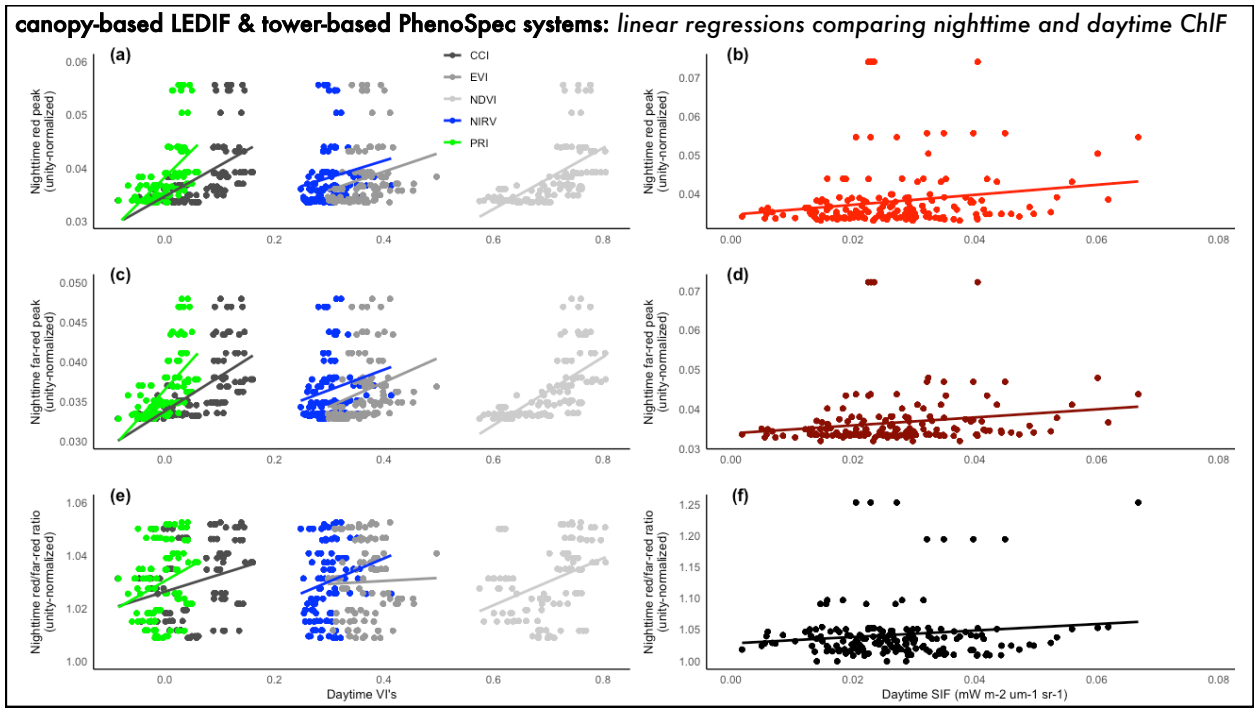

Figure 9: Linear relationships between nighttime results yielded from the canopy-based LEDIF system and daytime results from the tower-based PhenoSpec system. The relationships between the nighttime red peaks are compared with daytime (a) vegetation indices and (b) SIF, with the same comparisons for the far-red peaks (c,d) and red/far-red ratios (e,f). All nighttime results shown are from the Flame spectrometer with unity-based normalization.

Daily averages of GPP compared with daytime PhenoSpec results are displayed in *Figure 10*. Conversely, the linear relations between GPP and reflectance-based vegetation indices were much stronger compared to result of the LEDIF system. Explained variance between the PhenoSpec derived vegetation indices and eddy covariance derived GPP as multiple r-squared and p-values are as follows: NDVI = 0.48, p < 0.001; NIRv = 0.05, p < 0.001; PRI = 0.35, p < 0.001; CCI = 0.47, p < 0.001; EVI = 0.33, p < 0.001. Despite strong correlations between

reflectance-based and GPP products, the relationship between GPP and SIF yielded values as $R^2 = 0.07$ and $p < 0.001$.

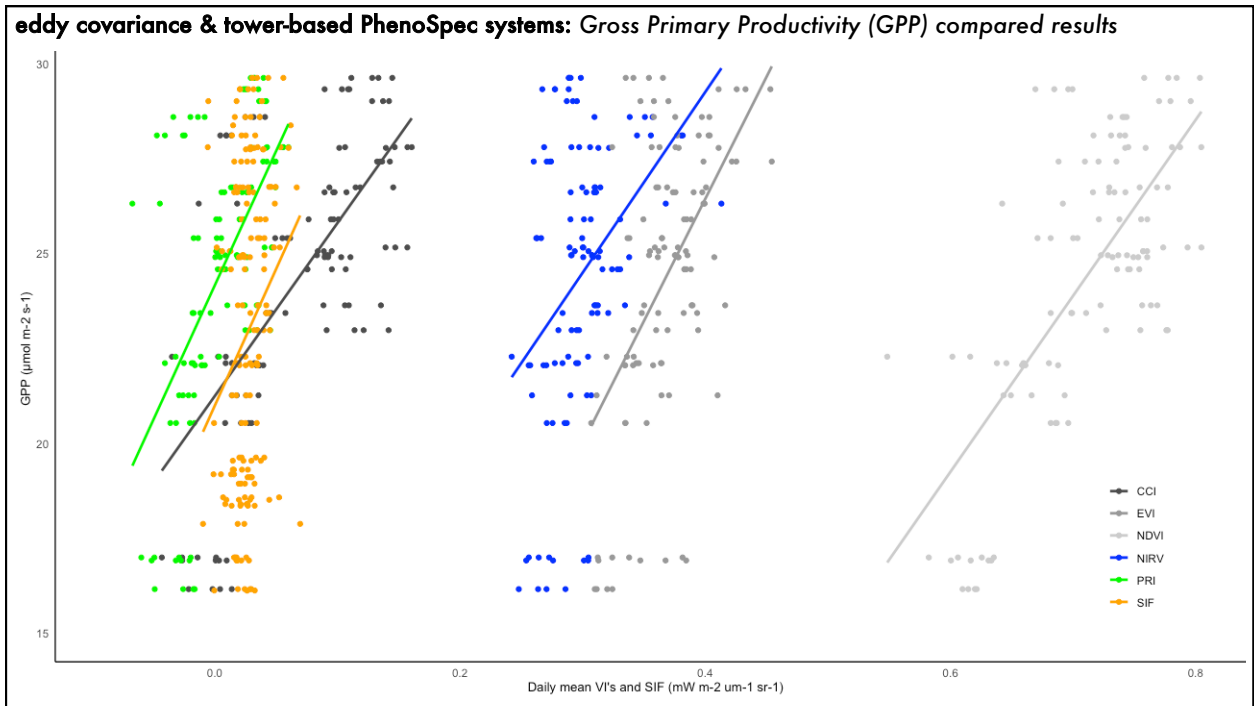

Figure 10: Linear relationships between the VIs and SIF derived from the tower-based PhenoSpec system and GPP derived from the eddy covariance system.

Random forest models for tower-based PhenoSpec and eddy covariance systems

To identify the contributions of different environmental parameters as drivers of GPP, importance for individual variables were assessed using random forest analyses for both entire observational period (EOP; *Figure 11*) and intensive-drought operational period (IOP; *Figure 12*) scenarios. With measured GPP as the response variable in all training simulations, the three scenarios differ in the predictor variables used to assess relative importance in relationship to GPP. Three random forest simulations were assessed for each of the EOP and IOP scenarios (six in total): spectral predictor variables from the PhenoSpec system (*Figure 11a/12a*), meteorological predictor variables from the eddy covariance system (*Figure 11b/12b*), and spectral and meteorological variables from both (*Figure 11c/12c*). For the spectral scenarios of

both the EOP (*Figure 11a*) and IOP, SIF was a primary driving variable ranked above the reflectance-based indices. Understandably, the EOP spectral scenario had higher accuracy compared to the IOP given the larger sample size, with their respective percentage of variance explained being 51 and 7 percent. For the combined spectral and meteorological scenarios of the EOP (*Figure 11b/c*), the meteorological predictor variables showed greater importance compared against the spectral variables. Latent heat flux, vapor pressure deficit, and air temperature showed high importance for the meteorological and combined scenarios for the EOP; however, SIF and the vegetation indices demonstrated lower importance for the combined scenarios. The meteorological variables outperformed the spectral variables for the IOP scenarios as well with latent heat flux, relative humidity, and ambient air pressure demonstrating high importance with 97 percent of model variance explained.

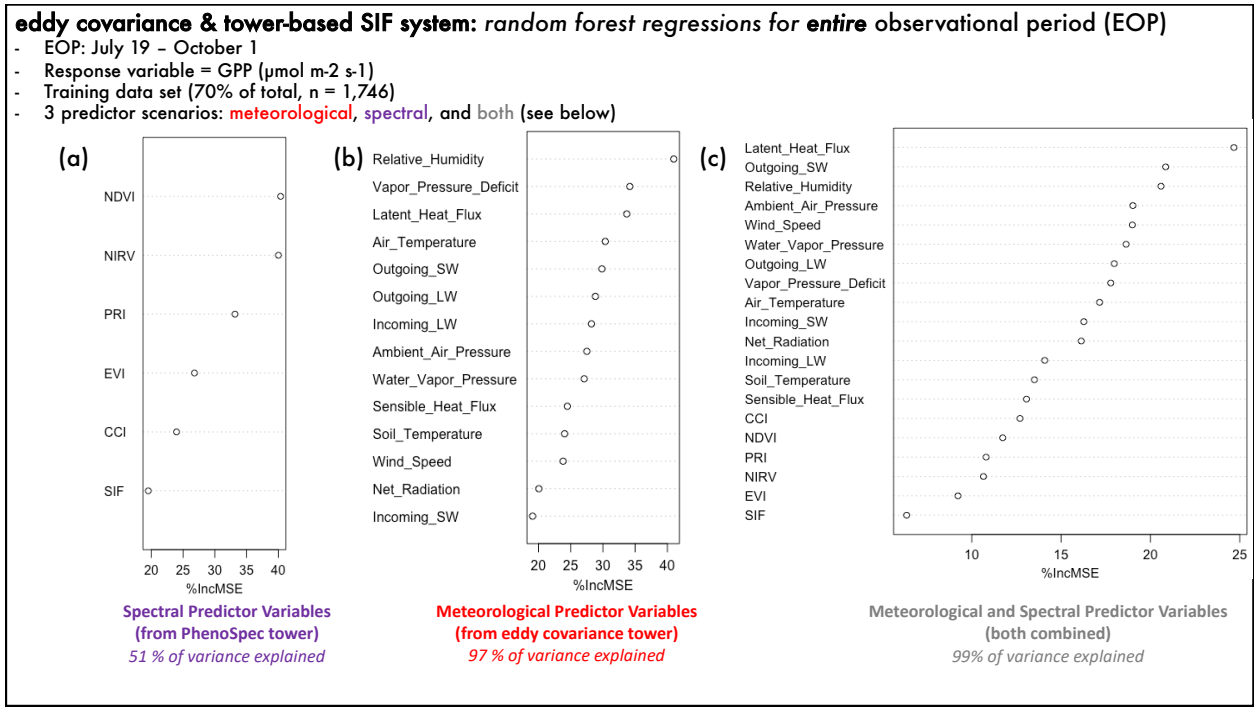

Figure 11: Random forest regressions with GPP as the response variable to (a) spectral, (b) meteorological, and (c) both spectral and meteorological predictor variables for the EOP. All data were split into training and

testing data sets at 70 and 30 percent, respectively. Individual predictor variable importance for model performance is weighed as the percent increase of mean squared error.

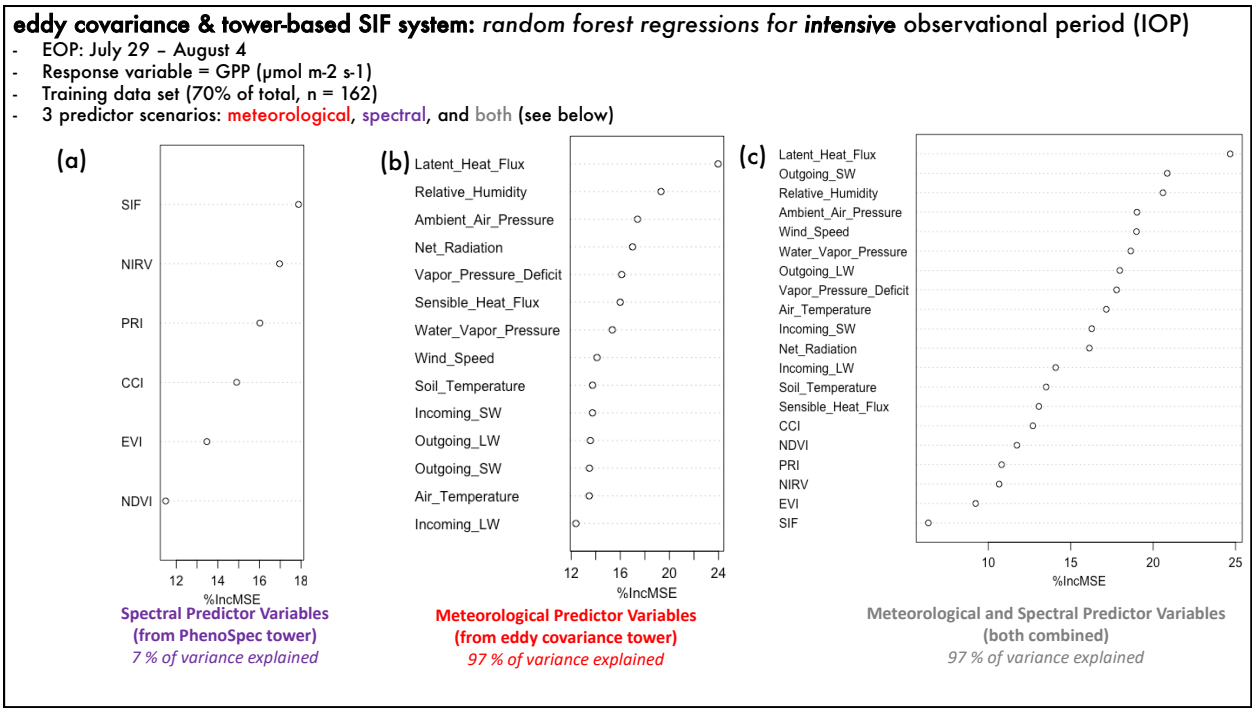

Figure 12: Random forest regressions with GPP as the response variable to (a) spectral, (b) meteorological, and (c) both spectral and meteorological predictor variables for the IOP.

To effectively test model performance, data from each EOP and IOP scenario were split into training (70 percent) and testing (30 percent) sets prior to running model simulations. The training data sets were used for assessing individual variable performance, while testing data were used to compared measured GPP to predicted GPP results output from the combined spectral and meteorological random forest models. *Figure 13* displays the linear relationship between eddy covariance system measured and random forest predicted GPP from (a) combined spectral and meteorological predictors and (b) just spectral predictors scenarios.

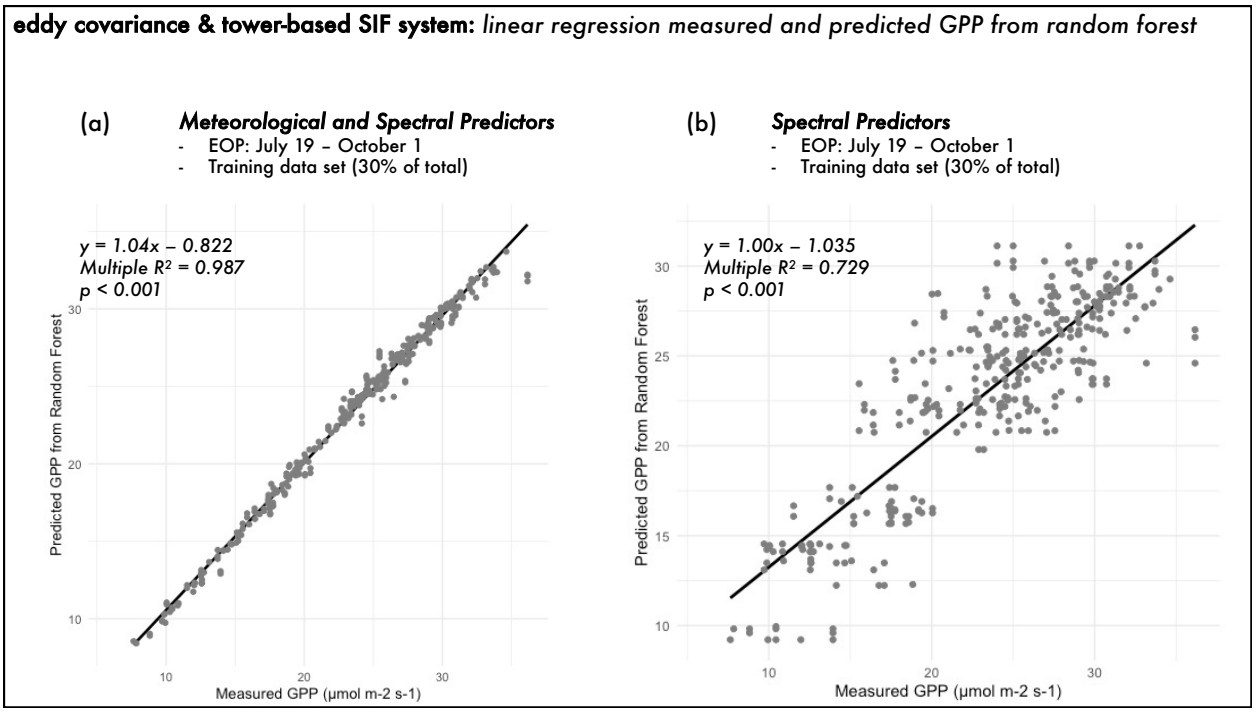

Figure 13: Measured GPP from eddy covariance system compared with predicted GPP from random forest models from (a) combined meteorological and spectral predictors and (b) just spectral predictors.

Discussion

Canopy-based LEDIF system

Design and setup takeaways

It was predetermined that the LEDIF system would be setup at the base of the tower at the field site so that it could have access to a constant AC power supply and be near the PhenoSpec system. Testing and necessary adjustments were made in the lab to ensure that the LEDs, timer, sensors, and spectrometers in the LEDIF system would operate as expected in normal field conditions. The primary objectives of lab testing prior to field deployment were to ensure that the LEDs operated properly on a digital timer outlet and that there was a distinguishable difference between LED and dark conditions recorded from the Apogee PAR sensor. While there was an observable difference in PAR between the LED and dark conditions with the LEDs positioned ~0.5 m from the Apogee sensor, PAR yields remained between 3-4 µmol * m-2 * s-1 for the duration of the study (*Supplemental Figure 3*).

Given that the Apogee Red/Far-Red sensor was the most affordable, low-cost option in the LEDIF system, we found that the Flame spectrometer operated through a Raspberry Pi 4 would offer midrange affordability and allow for more elaborate cross-comparisons to be made between the LEDIF and PhenoSpec systems. While the Apogee sensors offer the advantage of "plug-and-play" simplicity for iOS/Android users to record and extract data, the Raspberry Pi's Debian operating system required additional processes to allow for communication with the Flame spectrometer. The python-seabreeze (Poehlmann, 2019) module enables the Flame Vis-NIR spectrometer and many other Ocean Optics spectrometers to effectively communicate via python without the need for Mac/PC operating systems. Incorporating python-seabreeze allowed for the Flame spectrometer and Raspberry Pi 4 to communicate effectively and operate using

consistent measuring intervals throughout the study period. By positioning the Flame and Raspberry Pi 4 in a rugged weatherproof box, it was able to withstand external dust and hot temperatures. As suggested in Atherton *et al.* (2019), the LEDIF system measurements were taken from a fixed mounting point in continuous nightly operation to study seasonal dynamics and canopy-scale photosynthetic activity.

Data and results

The drastic peak in blue-excited emission spectra coinciding with the more subtle double-peaks in the red and far-red regions (*Figure 1d*) are supported by previous findings (Romero *et al.*, 2018; Atherton *et al.*, 2019). Both studies found that LED-induced spectra were weighted heavily towards the far-red region, resulting in particularly low red/far-red ratio values. However, in this experiment, the Apogee sensor (*Figure 4a/c/e*) revealed higher red emission values over those from the far-red. As a result, the red/far-red ratios for the Apogee sensor are quite high, especially for the non-normalized (*Figure 4b*) and blue-region normalized (*Figure 4d*). Similarly, the Flame spectra revealed higher red emission values compared to those from the far-red. These findings could differ given that previous studies yielded low red/far-red ratios using both pure blue-region LEDs (Romero *et al.*, 2018) and multispectral (Atherton *et al.*, 2019) light sources. This contrast could also be due to varying penetration characteristics of light depending on the medium; blue photons are typically absorbed closer to the top of the canopy while green, red, and far-red photons penetrate deeper (Vogelmann & Evans, 2002). Because the LEDIF system was positioned directly above a dense grapevine canopy, a greater portion of longer wavelength photons might have become reabsorbed or scattered within the canopy, and consequently undetected by the Apogee sensor or Flame spectrometer. While red photons are

more likely to be affected by chlorophyll reabsorption, escape of far-red photons depends more so on the structure of the canopy (Yang & van der Tol, 2018).

Corrections of raw spectra yielded from the Apogee Red/Far-Red sensor and Flame spectrometer through normalization was necessary due to the scattering and reabsorption of light photons, as advised in Romero *et* al. (2021). However, certain normalization methods displayed more consistency in detecting the subtle differences spectral intensities over others. For blue-region based methods, the raw output data from the Apogee Red/Far-Red sensor were normalized by respective Apogee PAR sensor measurements (*Supplemental Figure 3*), and raw output data from the Flame spectrometer were normalized by the mean intensities at the full-width at half maximum (FWHM) of the LED-induced blue peak (*Supplemental Figure 4*). While the daily averages for PAR from the Apogee sensor proved to be relatively consistent, individual measurements displayed high variability from one minute to the next. While this could possibly be a result of varying light conditions during the LED periods, it is more likely that the sensor picked up light as background noise, ultimately decreasing signal consistency. One potential solution to this issue would be to incorporate a structure to achieve isolated darkness during nighttime conditions for the LEDIF system without impeding noise from the environment. For blue region-based normalization of the Flame spectrometer, the raw results demonstrate a nearly identical trend of daily averages to those normalized by the FWHM intensities. Due to the particularly high raw intensity values observed from the blue peaks (~50k DN), any variability in the red and far-red intensities (~2k DN) were overshadowed by the drastic quotient between the two regions. As a result, there were no observable differences between the non-normalized raw output intensities and those normalized by the FWHM blue region-based method (*Figure 5b/c/d*).

However, unity-based normalization (*Supplemental Figure 5*) proved to be the most reasonable method for normalizing raw output red and far-red intensity measurements for both the Apogee sensor and Flame spectrometer. Arguably one of the more simplistic normalization methods, the unity-based approach offered consistency in utilizing respective minimum and maximum values for the red and far-red intensities. Thus, unlike blue region-based normalization, the unity-based approach ensured a fair comparison between the Apogee and Flame instruments. The Apogee sensor (*Figure 4f*) demonstrated modest intra-daily variation but generally remained inconsistent throughout the study period with a slight upward trend near the end. However, the Flame spectrometer (*Figure 5f*) displayed a decreasing trend spanning most of the study period except for an increase for a couple of days at the end of July near the beginning of the IOP. Although demonstrating slight dissimilarities between trends for non-normalized and normalized intensities of red peaks, far-red peaks, and red/far-red ratios, the Flame spectrometer proved more robust than the Apogee Red/Far-Red sensor. Most notably observed from raw measurements taken of the red and far-red intensities on an intra-daily (*Figure 3a/b*) basis and throughout the study period (*Figure 5a*), the Flame spectrometer demonstrates more consistent readings compared to the Apogee sensor (*Figure 3c/d; Figure 4a*).

As the novel approach, the LEDIF system is compared to the relatively established methodologies of SIF, GPP, and vegetation indices when characterizing unique phenomena of photosynthetic processes in this study. In observing time series of red and far-red spectral responses, a novel objective of this study was to compare fluorescence daily between daytime and nighttime conditions. Ultimately, the performance of the LEDIF system results are validated through such daily comparisons to illuminate broad trends and examine patterns of stress during the EOP and within the IOP. Because GPP, SIF, and reflectance-based indices derived from the

eddy covariance and PhenoSpec tower-based systems offer finer spatial and temporal resolutions for capturing spectra, trend comparisons between the two systems serve in this study as validation. Fluorescence measured between the three systems (LEDIF, PhenoSpec, eddy covariance) offers the ability to observe vegetation, detect change, and compared its trends under variable environmental conditions. Because there is not a real-time connection between the nighttime and daytime measurements of fluorescence, daily trends serve as the linkage between the two systems.

Strengths and limitations

We were motivated to explore nighttime LEDIF and build upon previous findings for a couple of reasons. Nighttime LEDIF offers a unique way to capture spectral emissions directly without interference from solar radiation that is inevitable during daytime conditions. By using LEDs emitting light at roughly 460 nm, the incoming light source is purely from the blue region; thus, eliminating any possibility of confounding influences from other regions of the spectrum as would be the case in any traditional daytime conditions with solar radiation as a light source. Another advantage of the LEDIF system is its cost affordability. A major motivation for originally designing and testing the LEDIF system was to assess its potential as a low-cost option for growers to monitor ChlF responses. The LEDIF system instruments consist of two price tiers, with the Apogee PAR and Red/Far-Red sensors being low cost (~$1k) and the Flame spectrometer being slightly higher ($3.5k). The tower-based PhenoSpec system costs (~$50k) and has higher operational costs for personnel and power demands as well. However, the LEDIF system has its limitations compared to the PhenoSpec system. While the LEDIF system offers the advantage of simplicity for both design, operations, and postprocessing, we are unable to quantify radiance and reflectance-based results without radiometric calibration. Because

nighttime data results are purely in ratio form (red peaks, far-red peaks, red far-red ratios), they are unitless and come at decreased spectral resolutions. Thus, nighttime results cannot be compared directly with daytime radiance and reflectance-based yields from the PhenoSpec system. Overall, the Flame spectrometer proved to have higher consistency for measurements recorded during nighttime conditions compared to those taken by the Apogee Red/Far-Red sensors. The major limitation of the Apogee Red/Far-Red sensor was its inability to measure consistently in both dark and LED periods, which may have been due to the system's overall design. The LEDIF system design could have been improved through installing more LEDs with higher wattage outputs. With such a weak PAR signal captured by the Apogee sensor throughout the study, an increased LED capacity could have allowed for higher signal-to-noise and instill greater confidence for measurement accuracy.

Tower-based PhenoSpec system

Design and setup takeaways

Unlike the canopy-based LEDIF system, the tower-based PhenoSpec system has been elaborately built on and tested in a variety of applications prior to this study (Grossman *et al*., 2018; Wong *et al.,* 2022). Specifically designed for high-throughput phenotyping, PhenoSpec was implemented in this study to capture spectral responses and variation in field subplots due to drought throughout a typical growing season. Except for the intensive observational period (IOP), the control and drought-induced subplots were treated with constant irrigation for the full duration of the study, or entire observational period (EOP). Thus, only during the IOP spanning July 29th through August 4th were irrigation patterns different between subplots. Target selection was planned such that a complete scanning cycle of all four subplots could be achieved within a half-hour period to match the sampling interval of the eddy covariance system. Thus, multiple

cycles of measurements were taken daily to ensure sufficient reflectance- and SIF-based results could be compared with those from the eddy covariance system.

Data and results compared with canopy-based LEDIF system

After implementing calibration coefficients to raw output data from the PhenoSpec system, radiance- and reflectance-based results were quantified and further examined (see Wong *et al*., *in review* for methodology). Post-calibration assessments of individual target measurements were necessary to ensure accurate representations of daily means, and such assessments were achieved through NDVI thresholding (*Supplemental Figure 2*) and filtering (*Supplemental Figure 5*) of drastically inaccurate measurements. Once having complete data sets for both PhenoSpec and eddy covariance tower systems – timeseries, linear comparisons and random forest regressions were ultimately conducted to identify the relationships between spectral results and determine their feasibility for predicting GPP. As for the timeseries results, GPP (*Figure 6h*) remains relatively stable at the beginning of the EOP before gradually declining starting around mid-August. Similar trends were demonstrated for some, but not all, results from PhenoSpec, displaying a gradual decline throughout the study period (*Figures 7/8*). In general, the reflectance-based indices and SIF demonstrated declining trends similar to that of GPP.

Linear comparisons revealed interesting relationships between the PhenoSpec, LEDIF, and eddy covariance systems. In a separate LEDIF study, Romero *et al*. (2021) examined linear relationships between primary productivity (ANPP) and passive remote sensing indicators and their correlation coefficients yielded adequate linear strength of the crop cultivars under examination. In a related study conducted one year prior at the same field site, Wong *et al.* (2022) found statistical significance in linear and detrended NDVI-GPP and PRI-GPP relationships. Reflectance-based indices and SIF have shown linear correlations with GPP in

other studies examining a single vegetation cover as well (Garbulsky *et al.*, 2013; Cai *et al.*, 2017). However, linear relations between the LEDIF and PhenoSpec systems revealed that there was little evidence for linearity between the two (*Figure 9*). This is not particularly surprising given the temporal disconnect between fluorescence being captured by two different systems for both daytime and nighttime conditions. However, daytime PhenoSpec system results yielded much higher explained variance in linear relations with GPP compared to nighttime LEDIF system results. While SIF accounted for only 7 percent of variance explained when compared with GPP, the reflectance-based indices showed a stronger performance (*Figure 10*).

Although the linear comparisons are useful in assessing simple relationships between two given parameters at a given point in time, random forest regressions were conducted for both the EOP and IOP to further interpret data complexities and determine parameter importance through a machine learning approach. By examining nonlinearities in the different parameters, the random forest approach enables a deeper understanding of seasonal variation between the between indices, SIF, GPP, and meteorological data (Chen *et al.*, 2021). With GPP as the response variable for all random forest models – spectral (PhenoSpec system) and meteorological (eddy covariance system) predictors were incorporated into the models for both EOP and IOP scenarios. While none of the meteorological predictor variables used in the model are utilized as products for quantifying GPP, their instantaneous measurements match temporally given the results are yielded from the same eddy covariance system. Overall, the meteorological predictor models outperform the spectral predictor models for both EOP and IOP scenarios, achieving 97 percent of model variance explained for both (*Figure 11b/12b*). From the spectral predictor models, the EOP and IOP scenarios were able to explain 51 and 6 percent of variance respectively with GPP as the response for both spectral predictor scenarios (*Figure 11a/12a*). In

support of the linear model results, NDVI outperformed the other reflectance-based indices and SIF in its ability to accurately predict GPP in the EOP scenario. The greenness- or structural-based NDVI may have outperformed the other indices due to its ability to detect degradation in chlorophyll and overall biomass over the growing season duration, which are common trajectories in grapevines (Peñuelas *et al.*, 1995; Zarco-Tejada *et al.*, 2012; Wong *et al.*, 2022).

While the reflectance-based indices were generally supportive of respective GPP measurements, it was surprising to find that SIF did not have the same success. To accurately represent SIF, it is important to consider all SIF-related processes: absorption, scattering, emission, and reabsorption (Porcar-Castell *et al.*, 2014b; Mohammed *et al.*, 2019). Because SIF and other PhenoSpec results are grouped based on the subplots surrounding the tower system, it is possible that certain environmental conditions might have contributed to inconsistencies in the overall SIF retrieval process. During initial data analyses, it became clear that there were occasionally SIF measurements well outside the expected value range, even during the midday window where retrieval conditions are optimal. As a result, subplot values were drastically divergent due to the influence of erroneous values (*Supplemental Figure 6*). Because many of these SIF measurements were well outside of the expected value range, a filter was placed to only include SIF values greater than -0.025 and less than 0.075 for the entire study. *Supplemental Figure 7* demonstrates these filtered SIF values as daily means used for all subsequent analyses (linear relationships and random forest models).

To address the dissimilarities in SIF results between subplots, unfiltered results were investigated, and subtle differences were found. While each subplot yielded similar SIF values in the first half of the study period – rip2 and rip4 demonstrated a decreasing trend for the latter half, while rip1 and rip3 daily means show divergence from a clear trend. Considering that rip2

and rip4 were located east of the tower, their decreasing trends correlate closely to that of GPP, whereas rip1 and rip3 do not. It is possible that these inconsistencies in the SIF signal for these two subplots (rip1 and rip3) were due to effects of scattering, shadowing, and angularity in the afternoon. Given that fluorescence measurements were quantified as daily means, variation in retrieved values during this duration can be partially attributed to changes in the proportion of shaded and sunlit leaves inside the canopy (Damm *et al.*, 2015; Biriukova *et al.*, 2020). In this study, the PhenoSpec instrument acquired target measurements consistently at an off-nadir angle, thus increasing error potential and inconsistencies between subplots due to the scattering of light and angularity of leaves. As a result, SIF will be more sensitive to angular issues than reflectance-based indices (Zeng *et al.*, 2022).

Because the scattering of light depends on the geometry of the sun and direction of observation from the top of the PhenoSpec tower (off-nadir), quantification of scattering is important to make meaningful comparisons between SIF observations retrieved under different solar and observation angles (Mohammed *et al.*, 2019). High SIF values from rip1 and rip3 are predominantly results of targets taken at high incident angles (eg. rip3_h1), while lower SIF values are observed at low incident angles (eg. rip3_l1). These inconsistencies in SIF values later in the summer growing season are potentially impacted by incident angularity given a lower sun angle, and thus, lower phase angle. Phase angle is measured as the angle between the sun-leaf incident and leaf-PhenoSpec incident for each target, and erroneous SIF values (particularly in rip1 and rip3) could be due to lower phase angularity later in the study period as summer approaches fall. Although its effects are worth considering, the quantification of phase angularity by target are beyond the scope of this study. Comprehensive efforts have been made to interpret scattering effects of light with respect to observation angle from the instrument and angularity of

the leaf (Köhler *et al.*, 2018; Liu *et al.*, 2019). Regarding the influence of directional scattering of fluorescence in the canopy, these studies have found that seasonality in SIF is affected by anisotropic angularity and subsequent corrections are needed. However, it should be noted that these studies utilize SIF derived from satellite-based platforms and implemented sophisticated machine-learning models to account for such angular effects.

It is also possible that variation in climatic conditions are responsible for a reasonable amount of the explained variance between SIF and GPP in random forest models (Chen *et al.*, 2021). However, given that this study maintained a relatively stable climate throughout the duration of the study (hot and dry conditions), it is less likely that climate contributed to the GPP and SIF variance. More predictor variables in a random forest simulation will most often improve model accuracy compared to less; and thus, the combination of spectral and meteorological predictors unsurprisingly yielded the highest amount of variance explained (*Figure 11c/12c*). In utilizing the testing data set partitioned prior to random forest model simulation, we were able to compare GPP predicted by the spectral predictor variables, as well as the combined spectral and meteorological predictors, with GPP measured from the eddy covariance system (*Figure 13*). Results from both the combined spectral and meteorological (*Figure 13a*) predictors, as well as those from purely spectral predictors (*Figure 13b*) yielded high linearity between measured and predicted GPP, with 99 and 73 percent of variance explained, respectively. This indicates that the random forest approach was successful in predicting GPP outcomes with new data using both the spectral and meteorological predictors.

Strengths and limitations

As a mobile derivative of PhotoSpec (Grossmann *et al.*, 2018b), the PhenoSpec system has been developed for multiple field seasons prior to its installation for this experiment and is

generally more familiar to our research team. There are three notable advantages of the PhenoSpec system when compared to the LEDIF system: spatial scale, radiometric calibration, and unit-based measurements. Compared to the LEDIF system, the vertically inclined PhenoSpec system offers greater spatial extent, thus allowing for more area coverage, controlled target selection, and autonomy for measuring spectra by subplot. Radiance, reflectance, and fluorescence were quantified from raw output spectral intensities of PhenoSpec instruments, but these results were made possible through radiometric calibration with the SVC spectroradiometer. The ability to calibrate and compare daytime spectra directly with the SVC spectroradiometer instills confidence in the PhenoSpec system's ability to measure accurately and assign units to otherwise unitless raw intensities of spectral characteristics.

This confidence was not shared with the LEDIF system due to its inability to conduct radiometric calibration or NDVI thresholding as a filtering process. Since the primary intention for the canopy-based system was to operate during nighttime conditions to capture ChlF, radiometric calibration and real-time comparisons with PhenoSpec and eddy covariance outputs were not an option. For this reason, normalizing approaches were implemented for (eg. unity-based, PAR, FWHM) raw data outputs of both the Apogee Red/Far-Red sensor and Flame spectrometer in the LEDIF system to capture seasonality and variation in trends. This enabled the quantification of daily trends and averages that could be compared between nighttime and daytime results. However, the PhenoSpec system is rather expensive in terms of personnel demands and overall price. Throughout the study period, the PhenoSpec system required daily monitoring via remote PC access to ensure its functionality and continuous operations, whereas the LEDIF system did not.

Assessment of project goals

The primary goals of this study were to: (a) determine the feasibility of implementing an affordable, easy to function ground-based remote sensing tool capable of capturing chlorophyll fluorescence properties within grape vineyard canopies through the implementation of blue LEDs and low-cost sensors at night, and (b) compare its results with other spectral and meteorological parameters indicative of plant physiological characteristics. While nighttime LEDIF is a relatively unconventional approach when compared to daytime SIF, it fundamentally offers a unique perspective through its active approach of inducing chlorophyll fluorescence. In such regard, our research team was successful in implementing an affordable, easy to function tool that we set out to do in the original project goals.

Although we were successful in deploying the instrument and capturing fluorescence as intended in the latter of the two overarching goals, there were some design caveats revealed during data analysis. Particularly, I found difficulty in comparing nighttime and daytime results directly given their temporal disconnect. Because the PhenoSpec and eddy covariance systems both operated exclusively during daytime conditions, direct linkages between their measurements could be made. Because there is not necessarily a real-time, diurnal linkage between the LEDIF and PhenoSpec results, it was challenging to extrapolate relationships without oversimplifying phenological phenomena. Thus, half-hourly and hourly comparisons could not be made between nighttime and daytime results. It is for this reason that all nighttime and daytime normalized, and calibrated results shown were quantified as daily means for their respective light conditions.

It is important to note that, throughout this study, we have discussed cost and affordability based on a fiscal price. While our assessment of what constitutes as “affordable” is

completely subjective, this study can hopefully provide some insight as to the range of costs to undergo such a study and performance capabilities of the instruments used. Both the LEDIF and PhenoSpec systems, as well as the instruments comprised within, are useful in their own ways; however, their utility depends entirely on the needs of the user's spectral, spatial, and fiscal demands. The PhenoSpec system offers a much spatial extent, finer spectral capabilities, and ultimately shows great promise for high-throughput phenotyping (Wong *et al*. *in review*). While the LEDIF system could be perceive as immature compared to the PhenoSpec in this study, the idea of nighttime fluorescence offers great potential for its application towards plant sciences in general. Although this study nor any one alone can prove the worth of LEDIF, its conception as a low-cost alternative for quantifying chlorophyll fluorescence offers hope for its future development.

Conclusion

Through the implementation of tower-based and canopy-based remote sensing systems, this study aims to assess their unique capabilities for tracking drought stress and seasonality at a grape vineyard in California. In comparing spectral results acquired through these remote sensing systems with GPP results acquired through an eddy covariance platform, we can monitor the fate of solar energy to better understand environmental phenomena and photosynthetic processes. While traditional methods for quantifying reflectance-based vegetation indices, SIF, and GPP have shown immense potential for detecting physiological stress and seasonality, we furthered this effort and deployed a low-cost alternative for measuring chlorophyll fluorescence at night (LEDIF). The canopy-based, nighttime LEDIF system used in this study was successful in measuring a "pure" fluorescence signal unaffected by the associative influences of daytime solar radiation. This study demonstrates the growing potential for seasonal applications of such remote sensing tools to provide automated, continuous, and real-time data for tracking variation in GPP and drought stress.

Impeding drought-stress in California due to climate change has emerged as a prominent issue for agricultural production in the twenty-first century. California is a global hub for a variety of specialty crops, with grapes continuously ranking as state's top in terms of production and value. Along with many other crops grown in the state, grapes demonstrate moderately high sensitivity to projected mid-century changes in temperature (Kerr *et al.*, 2018). In a region prone to extensive periods of drought, meticulous irrigation management is essential for both crop longevity and overall water conservation in California. This study implements remotely sensed measurements of reflectance (NDVI, CCI, PRI, etc.), chlorophyll fluorescence (SIF/LEDIF), and gross primary productivity (GPP) to characterize spectral responses throughout a growing season

at a Merlot grape vineyard in California's Central Valley. Through capturing chlorophyll fluorescence and other dynamic physiological data during an intensive observational period (IOP) of drought induction, this work aims to help growers and managers to achieve precise irrigation and mitigate the adverse effects of climate change on grape production.

Supplemental Figures

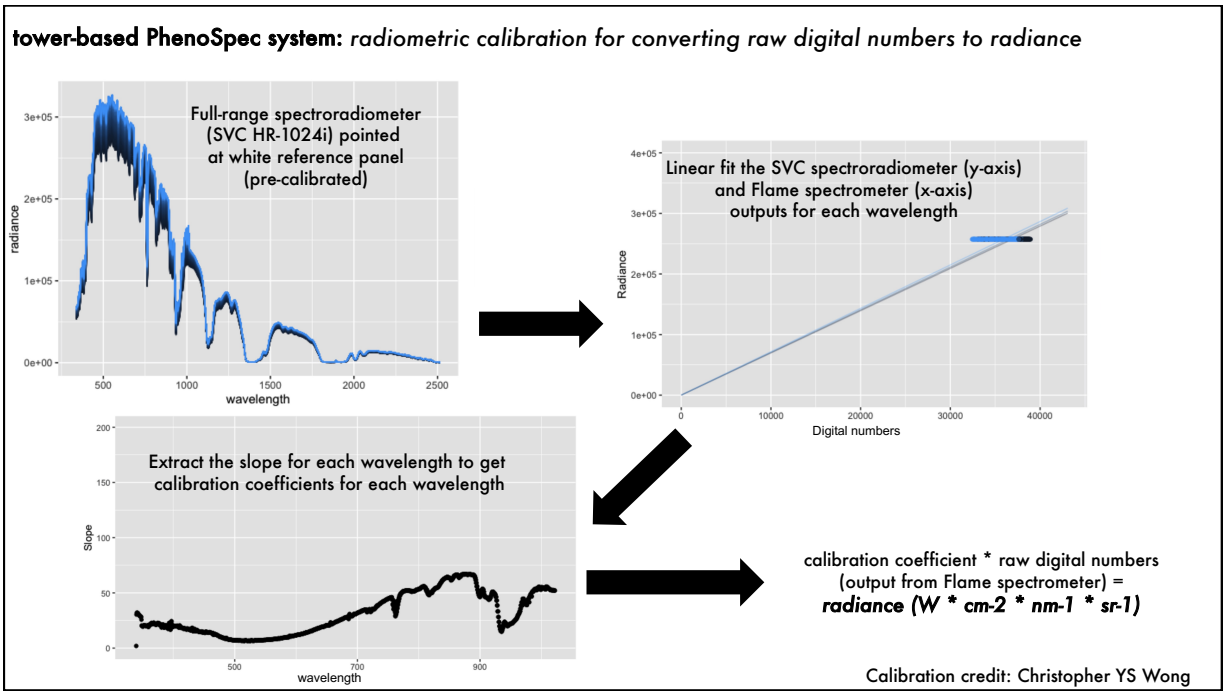

Supplemental Figure 1: Process for converting raw digital numbers to radiance from the tower-based PhenoSpec system spectrometers.

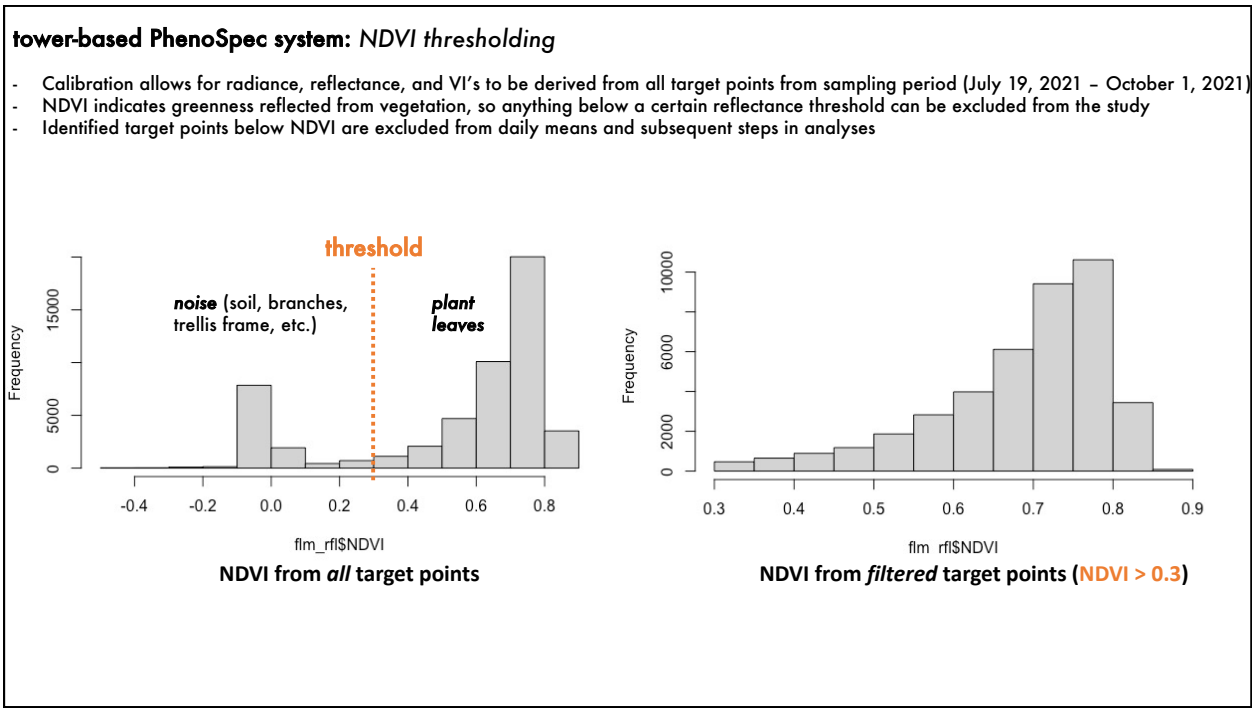

Supplemental Figure 2: Normalized difference vegetation index (NDVI) thresholding used to differentiate vegetation from non-vegetation sample points yielded from the tower-based PhenoSpec system.Threshold is set to exclude all sample points where NDVI < 0.30 while retaining values greater than.

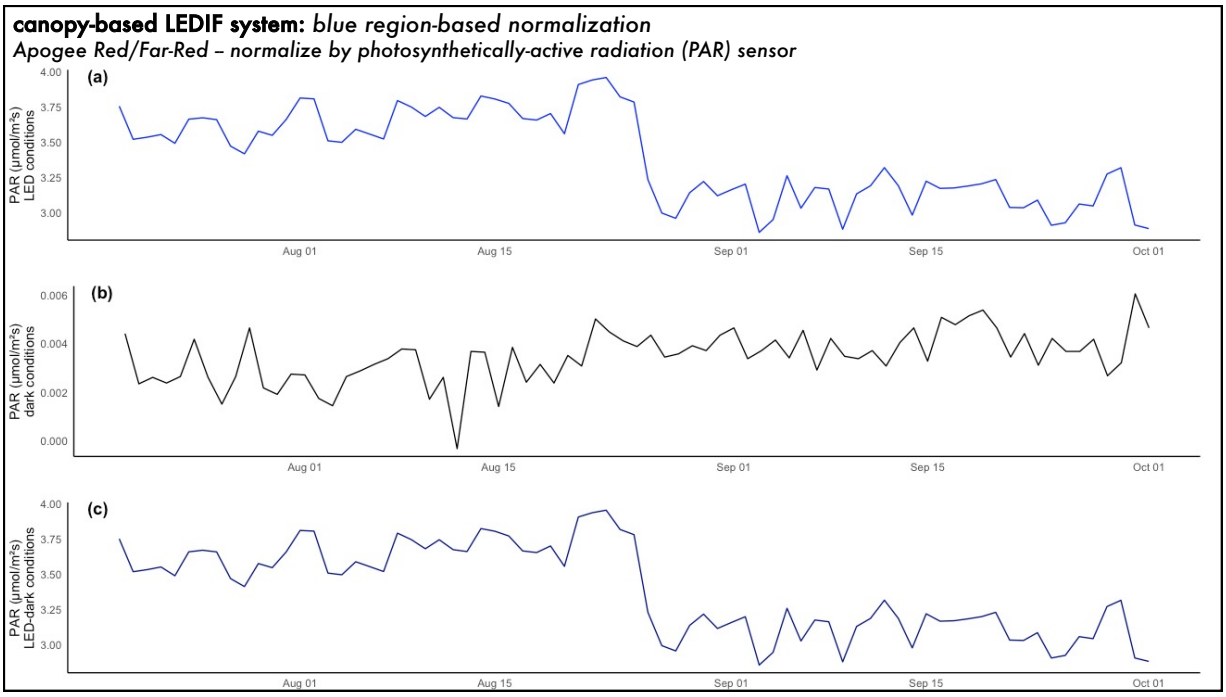

Supplemental Figure 3: Photosynthetically-active radiation signal for (a) LED, (b) dark, and (c) the difference between LED and dark periods from the Apogee PAR sensor. PAR values are used to normalize red and far-red peaks from the Apogee Red/Far-Red sensor for blue-region based normalization.

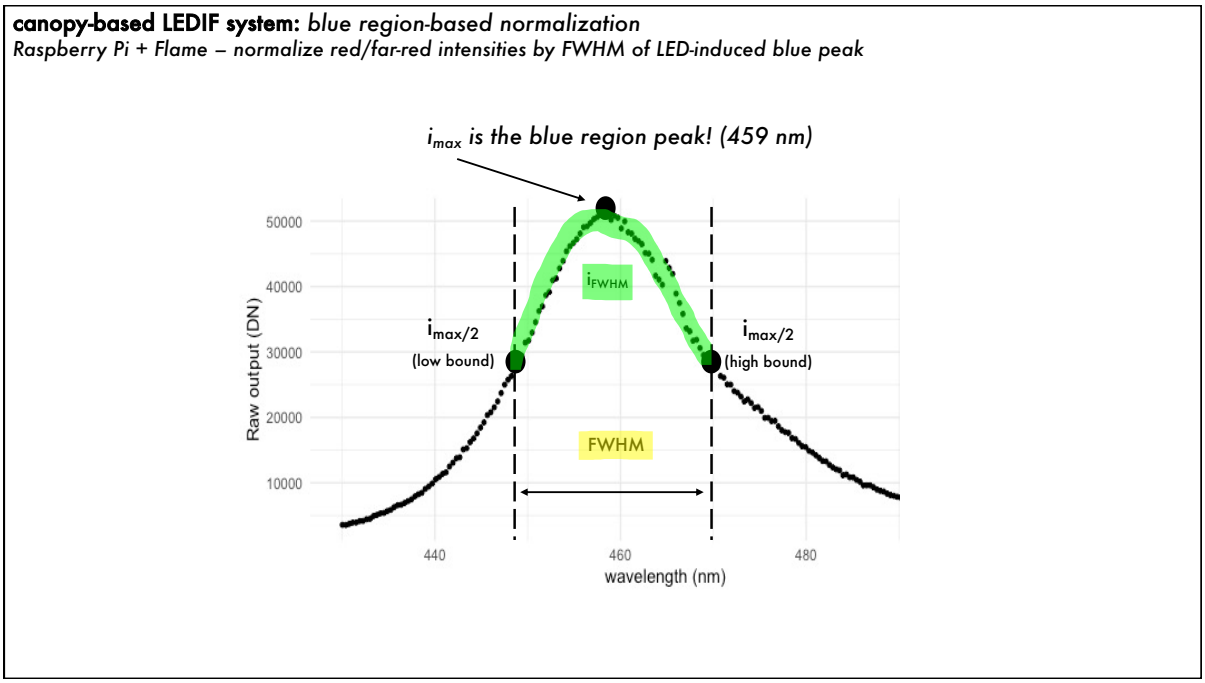

Supplemental Figure 4: Blue-region spectral peak from the Flame spectrometer of the canopy-based LEDIF system during LED periods. Labels indicate spectral peak at maximum intensities (i_{max}), half-maximum intensities at low and high bounds of the blue peak ($i_{max/2}$), the full-width at half maximum (FWHM), and the mean intensity within the FWHM range (i_{FWHM}). i_{FWHM} values are used to normalize red and far-red peaks from the Flame spectrometer for blue-region based normalization.

canopy-based LEDIF system: *unity-based normalization*
Raspberry Pi + Flame & Apogee: normalize red/far-red intensities by respective minimum and maximum values

$$i' = \frac{i - i_{min}}{i_{max} - i_{min}}$$

unity-based normalized intensities (i') calculated for each measurement sampled in the red and far-red regions

Supplemental Figure 5:Unity-based normalization formula used to normalize red and far-red intensities by respective minimum and maximum values. Unity-based normalizations are used to normalize data from both the Apogee Red/Far-Red sensor and Flame spectrometer.

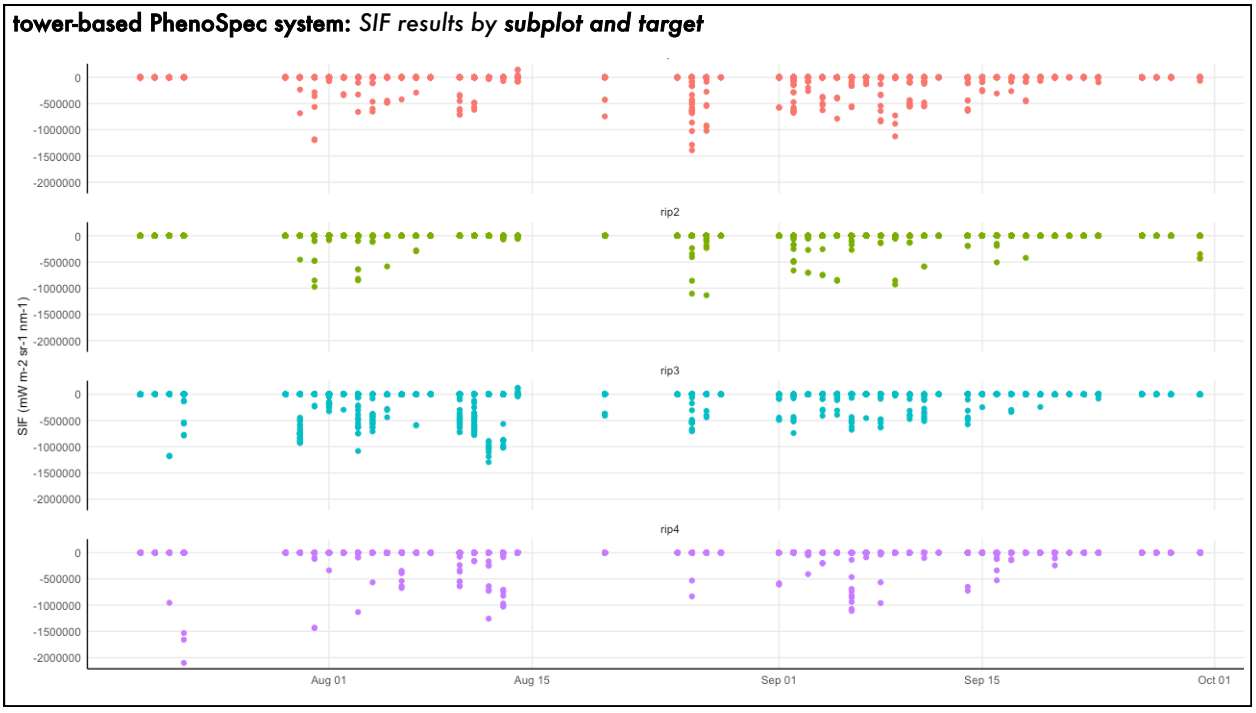

Supplemental Figure 6: Timeseries of unfiltered SIF results based by subplot

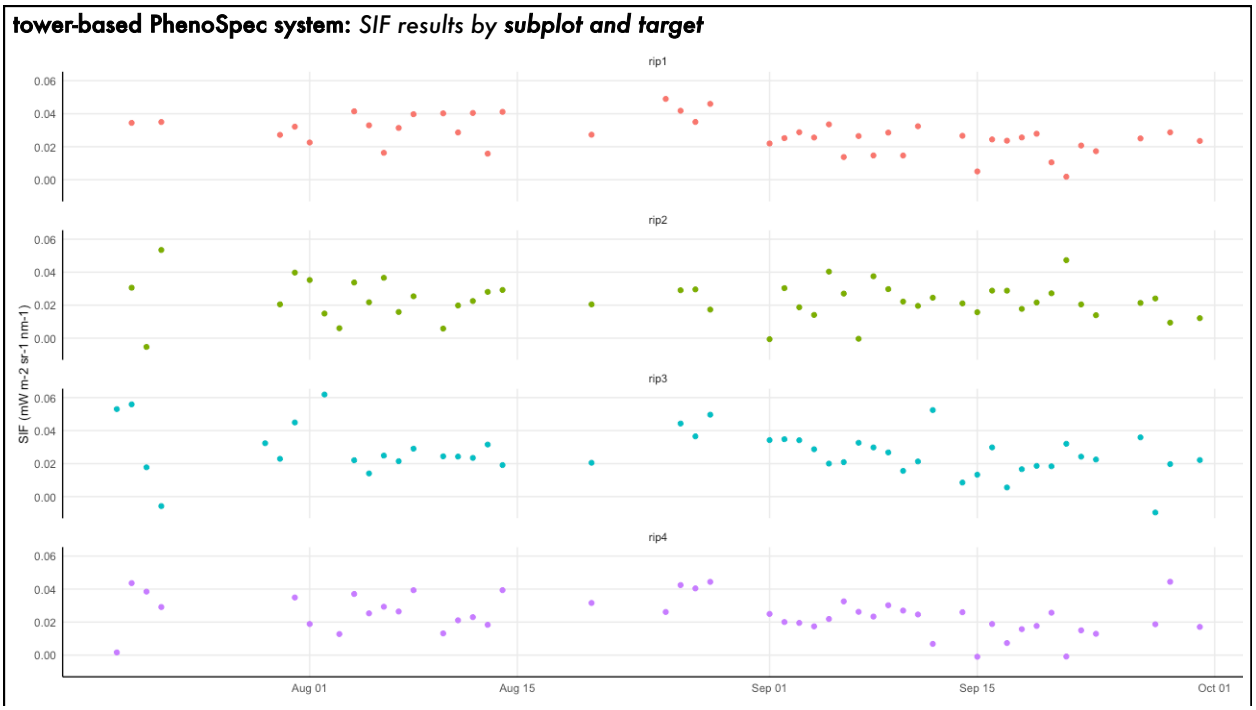

Supplemental Figure 7: Timeseries of filtered SIF daily means results by subplot (-0.025 < SIF < 0.075)

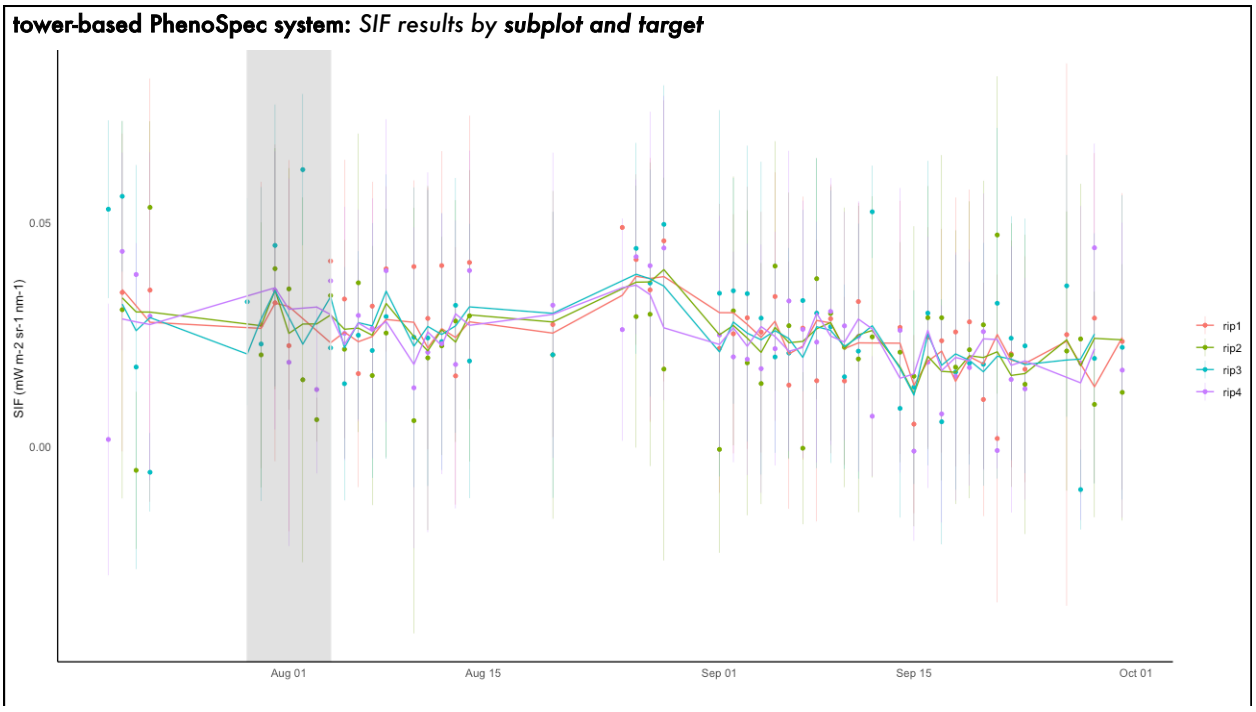

Supplemental Figure 8: SIF dail means and standard deviations grouped by subplot. Trendlines represent daily mean values of SIF, while the points and vertical lines represent standard deviations by day.

References

Atherton J, Liu W, Porcar-Castell A. **2019**. Nocturnal Light Emitting Diode Induced Fluorescence (LEDIF): A new technique to measure the chlorophyll a fluorescence emission spectral distribution of plant canopies in situ. *Remote Sensing of Environment* **231**: 111137.

Badgley G, Field CB, Berry JA. **2017**. Canopy near-infrared reflectance and terrestrial photosynthesis. *Science Advances* **3**.

Baker NR. **2008**. Chlorophyll fluorescence: A probe of photosynthesis in vivo. *Annual Review of Plant Biology* **59**: 89–113.

Biriukova K, Celesti M, Evdokimov A, Pacheco-Labrador J, Julitta T, Migliavacca M, Giardino C, Miglietta F, Colombo R, Panigada C, *et al.* 2020. Effects of varying solar-view geometry and canopy structure on solar-induced chlorophyll fluorescence and PRI. *International Journal of Applied Earth Observation and Geoinformation* **89**: 102069.

Brissette L, Wong CY, McHugh DP, Klein M, Au J, Orcutt E, Magney T. Tracking the temporal dynamics of canopy-scale chlorophyll fluorescence with a low-cost nighttime LED platform. *Manuscript in preparation*.

Butler WL. **2003**. Energy Distribution in the Photochemical Apparatus of Photosynthesis. *http://dx.doi.org/10.1146/annurev.pp.29.060178.002021* **29**: 345–378.

Cai Z, Jönsson P, Jin H, Eklundh L. **2017**. Performance of Smoothing Methods for Reconstructing NDVI Time-Series and Estimating Vegetation Phenology from MODIS Data. *Remote Sensing 2017, Vol. 9, Page 1271* **9**: 1271.

Chang CY, Guanter L, Frankenberg C, Köhler P, Gu L, Magney TS, Grossmann K, Sun

Y. **2020**. Systematic assessment of retrieval methods for canopy far-red solar-induced chlorophyll fluorescence using high-frequency automated field spectroscopy. *Wiley Online Library* **125**.

Chen A, Mao J, Ricciuto D, Lu D, Xiao J, Li X, Thornton PE, Knapp AK. **2021**. Seasonal changes in GPP/SIF ratios and their climatic determinants across the Northern Hemisphere. *Global Change Biology* **27**: 5186–5197.

Damm A, Guanter L, Verhoef W, Schläpfer D, Garbari S, Schaepman ME. **2015**. Impact of varying irradiance on vegetation indices and chlorophyll fluorescence derived from spectroscopy data. *Remote Sensing of Environment* **156**: 202–215.

Frankenberg C, Berry J. **2017**. *Solar induced chlorophyll fluorescence: Origins, relation to photosynthesis and retrieval*. Elsevier.

Frankenberg C, Fisher JB, Worden J, Badgley G, Saatchi SS, Lee JE, Toon GC, Butz A, Jung M, Kuze A, *et al.* 2011. New global observations of the terrestrial carbon cycle from GOSAT: Patterns of plant fluorescence with gross primary productivity. *Geophysical Research Letters* **38**.

Gamon JA, Huemmrich KF, Wong CYS, Ensminger I, Garrity S, Hollinger DY, Noormets A, Peñuelask J. **2016**. A remotely sensed pigment index reveals photosynthetic phenology in evergreen conifers. *Proceedings of the National Academy of Sciences of the United States of America* **113**: 13087–13092.

Gamon J, Penuelas J, environment CF-RS of, 1992 undefined. A narrow-waveband spectral index that tracks diurnal changes in photosynthetic efficiency. *Elsevier*.

Gamon JA, Serrano L, Surfus JS. **1997**. The photochemical reflectance index: An optical

indicator of photosynthetic radiation use efficiency across species, functional types, and nutrient levels. *Oecologia* **112**: 492–501.

Garbulsky M, Peñuelas J, … RO-I journal of, 2013 undefined. **2013**. Leaf and stand-level carbon uptake of a Mediterranean forest estimated using the satellite-derived reflectance indices EVI and PRI. *Taylor & Francis* **34**: 1282–1296.

Gitelson AA, Buschmann C, Lichtenthaler HK. **1998**. Leaf chlorophyll fluorescence corrected for re-absorption by means of absorption and reflectance measurements. *Journal of Plant Physiology* **152**: 283–296.

Grossmann K, Frankenberg C, Magney TS, Hurlock SC, Seibt U, Stutz J. **2018a**. PhotoSpec: A new instrument to measure spatially distributed red and far-red Solar-Induced Chlorophyll Fluorescence.

Grossmann K, Frankenberg C, Magney TS, Hurlock SC, Seibt U, Stutz J. **2018b**. PhotoSpec: A new instrument to measure spatially distributed red and far-red Solar-Induced Chlorophyll Fluorescence. *Remote Sensing of Environment* **216**: 311–327.

Guanter L, Rossini M, Colombo R, Meroni M, Frankenberg C, Lee JE, Joiner J. **2013**. Using field spectroscopy to assess the potential of statistical approaches for the retrieval of sun-induced chlorophyll fluorescence from ground and space. *Remote Sensing of Environment* **133**: 52–61.

Hák R, Lichtenthaler HK, Rinderle U. **1990**. Decrease of the chlorophyll fluorescence ratio F690/F730 during greening and development of leaves. *Radiation and Environmental Biophysics 1990 29:4* **29**: 329–336.

Huete A, Didan K, Miura T, Rodriguez E, … XG-R sensing of, 2002 U. **2002**. Overview of

the radiometric and biophysical performance of the MODIS vegetation indices. *Elsevier* **83**: 195–213.

Kerr A, Dialesandro J, Steenwerth K, Lopez-Brody N, Elias E. **2018**. Vulnerability of California specialty crops to projected mid-century temperature changes. *Climatic Change* **148**: 419–436.

Knyazikhin Y, Martonchik J V., Myneni RB, Diner DJ, Running SW. **1998**. Synergistic algorithm for estimating vegetation canopy leaf area index and fraction of absorbed photosynthetically active radiation from MODIS and MISR data. *Journal of Geophysical Research: Atmospheres* **103**: 32257–32275.

Köhler P, Frankenberg C, Magney TS, Guanter L, Joiner J, Landgraf J. **2018**. Global Retrievals of Solar-Induced Chlorophyll Fluorescence With TROPOMI: First Results and Intersensor Comparison to OCO-2. *Geophysical Research Letters* **45**: 10,456-10,463.

Kustas WP, Anderson MC, Alfieri JG, Knipppper K, Torres-Rua A, Parry CK, Nieto H, Agam N, White WA, Gao F, *et al.* 2018. The grape remote sensing atmospheric profile and evapotranspiration experiment. *Bulletin of the American Meteorological Society* **99**: 1791–1812.

Liaw, A., & Wiener, M. 2002. Classification and regression by randomForest. *R news* **23**: 18-22.

Liu X, Guanter L, Liu L, Damm A, Malenovský Z, Rascher U, Peng D, Du S, Gastellu-Etchegorry JP. **2019**. Downscaling of solar-induced chlorophyll fluorescence from canopy level to photosystem level using a random forest model. *Remote Sensing of Environment* **231**.

Magney TS, Barnes ML, Yang X. **2020**. On the Covariation of Chlorophyll Fluorescence and Photosynthesis Across Scales. *Geophysical Research Letters* **47**: e2020GL091098.

Magney TS, Bowling DR, Logan BA, Grossmann K, Stutz J, Blanken PD, Burns SP, Cheng R, Garcia MA, Köhler P, *et al.* 2019. Mechanistic evidence for tracking the seasonality of photosynthesis with solar-induced fluorescence. *Proceedings of the National Academy of Sciences* **116**: 11640–11645.

Magney TS, Frankenberg C, Fisher JB, Sun Y, North GB, Davis TS, Kornfeld A, Siebke K. **2017**. Connecting active to passive fluorescence with photosynthesis: a method for evaluating remote sensing measurements of Chl fluorescence. *New Phytologist* **215**: 1594–1608.

Maxwell K, Johnson GN. **2000**. Growth and Physiological Performance of Aerobic and Lowland Rice as Affected by Water Stress at Selected Growth Stages. *Journal of Experimental Botany* **51**: 659–668.

Meroni M, Rossini M, Guanter L, Alonso L, Rascher U, Colombo R, Moreno J. **2009**. Remote sensing of solar-induced chlorophyll fluorescence: Review of methods and applications. *Remote Sensing of Environment* **113**: 2037–2051.

Mohammed GH, Colombo R, Middleton EM, Rascher U, van der Tol C, Nedbal L, Goulas Y, Pérez-Priego O, Damm A, Meroni M, *et al.* 2019. Remote sensing of solar-induced chlorophyll fluorescence (SIF) in vegetation: 50 years of progress. *Remote Sensing of Environment* **231**: 111177.

Myneni RB, Williams DL. **1994**. On the relationship between FAPAR and NDVI. *Remote Sensing of Environment* **49**: 200–211.

Papageorgiou G. **2004**. *Chlorophyll a fluorescence: a signature of photosynthesis*.

Peñuelas J, Filella I, Gamon JA. **1995**. Assessment of photosynthetic radiation-use efficiency with spectral reflectance. *New Phytologist* **131**: 291–296.

Pettorelli N, Vik JO, Mysterud A, Gaillard JM, Tucker CJ, Stenseth NC. **2005**. Using the satellite-derived NDVI to assess ecological responses to environmental change. *Trends in Ecology & Evolution* **20**: 503–510.

Poehlmann, A. 2019. python-seabreeze. https://python-seabreeze.readthedocs.io/en/latest/index.html.

Porcar-Castell A. **2011**. A high-resolution portrait of the annual dynamics of photochemical and non-photochemical quenching in needles of Pinus sylvestris. *Physiologia Plantarum* **143**: 139–153.

Porcar-Castell A, Malenovský Z, Magney T, Van Wittenberghe S, Fernández-Marín B, Maignan F, Zhang Y, Maseyk K, Atherton J, Albert LP, *et al.* 2021. Chlorophyll a fluorescence illuminates a path connecting plant molecular biology to Earth-system science. *Nature Plants* **7**: 998–1009.

Porcar-Castell A, Tyystjärvi E, Atherton J, Van Der Tol C, Flexas J, Pfündel EE, Moreno J, Frankenberg C, Berry JA. **2014a**. Linking chlorophyll a fluorescence to photosynthesis for remote sensing applications: Mechanisms and challenges. *Journal of Experimental Botany* **65**: 4065–4095.

Porcar-Castell A, Tyystjärvi E, Atherton J, Van Der Tol C, Flexas J, Pfündel EE, Moreno J, Frankenberg C, Berry JA. **2014b**. Linking chlorophyll a fluorescence to photosynthesis for remote sensing applications: Mechanisms and challenges. *Journal of*

Experimental Botany **65**: 4065–4095.

R Development Core Team. 2020. R: A Language and Environment for Statistical Computing. http://www.r-project.org/.

Rajewicz PA, Atherton J, Alonso L, Porcar-Castell A. **2019**. Leaf-Level Spectral Fluorescence Measurements: Comparing Methodologies for Broadleaves and Needles. *Remote Sensing 2019, Vol. 11, Page 532* **11**: 532.

Romero JM, Cordon GB, Lagorio MG. **2018**. Modeling re-absorption of fluorescence from the leaf to the canopy level. *Remote Sensing of Environment* **204**: 138–146.

Romero JM, Otero A, Lagorio MG, Berger AG, Cordon GB. **2021**. Canopy active fluorescence spectrum tracks ANPP changes upon irrigation treatments in soybean crop. *Remote Sensing of Environment* **263**: 112525.

Schotanus P, Nieuwstadt FTM, De Bruin HAR. **1983**. Temperature measurement with a sonic anemometer and its application to heat and moisture fluxes. *Boundary-Layer Meteorology 1983 26:1* **26**: 81–93.

Tucker CJ. **1979**. *Red and Photographic Infrared Linear Combinations for Monitoring Vegetation*.

Turner AJ, Köhler P, Magney TS, Frankenberg C, Fung I, Cohen RC. **2020**. A double peak in the seasonality of California's photosynthesis as observed from space. *Biogeosciences* **17**: 405–422.

Vogelmann TC, Evans JR. **2002**. Profiles of light absorption and chlorophyll within spinach leaves from chlorophyll fluorescence. *Plant, Cell and Environment* **25**: 1313–1323.

Webb EK, Pearman GI, Leuning R. **1980**. Correction of flux measurements for density effects due to heat and water vapour transfer. *Quarterly Journal of the Royal Meteorological Society* **106**: 85–100.

Wong CYS, Bambach NE, Alsina MM, McElrone AJ, Jones T, Buckley TN, Kustas WP, Magney TS. **2022**. Detecting short-term stress and recovery events in a vineyard using tower-based remote sensing of photochemical reflectance index (PRI). *Irrigation Science* **1**: 1–14.

Wong CYS, Gamon JA. **2015a**. Three causes of variation in the photochemical reflectance index (PRI) in evergreen conifers. *New Phytologist* **206**: 187–195.

Wong CYS, Gamon JA. **2015b**. The photochemical reflectance index provides an optical indicator of spring photosynthetic activation in evergreen conifers. *New Phytologist* **206**: 196–208.

Wong CYS, McHugh DP, Jones T, Gilbert ME, Gepts P, Buckley TN, Magney TS. Mobile tower-based remote sensing enables continuous high-throughput phenotyping of vegetation physiology. *Manuscript in review*.

Yang X, Tang J, Mustard JF, Lee JE, Rossini M, Joiner J, Munger JW, Kornfeld A, Richardson AD. **2015**. Solar-induced chlorophyll fluorescence that correlates with canopy photosynthesis on diurnal and seasonal scales in a temperate deciduous forest. *Geophysical Research Letters* **42**: 2977–2987.

Yang P, van der Tol C. **2018**. Linking canopy scattering of far-red sun-induced chlorophyll fluorescence with reflectance. *Remote Sensing of Environment* **209**: 456–467.

Zarco-Tejada PJ, González-Dugo V, Berni JAJ. **2012**. Fluorescence, temperature and narrow-

band indices acquired from a UAV platform for water stress detection using a micro-hyperspectral imager and a thermal camera. *Remote Sensing of Environment* **117**: 322–337.

Zeng Y, Hao D, Huete A, Dechant B, Berry J, Chen JM, Joiner J, Frankenberg C, Bond-Lamberty B, Ryu Y, *et al.* 2022. Optical vegetation indices for monitoring terrestrial ecosystems globally. *Nature Reviews Earth and Environment* **3**: 477–493.